

Sequential- and Parallel- Constrained Max-value Entropy Search via Information Lower Bound

Shion Takeno^{1,2}, Tomoyuki Tamura¹, Kazuki Shitara^{3,4}, and Masayuki Karasuyama¹

¹Nagoya Institute of Technology

²RIKEN Center for Advanced Intelligence Project

³Osaka University

⁴Japan Fine Ceramics Center

*takeno.s.mllab.nit@gmail.com, tomoyuki.tamura@nitech.ac.jp,
shitara@jwri.osaka-u.ac.jp, karasuyama@nitech.ac.jp*

Abstract

Max-value entropy search (MES) is one of the state-of-the-art approaches in Bayesian optimization (BO). In this paper, we propose a novel variant of MES for constrained problems, called Constrained MES via Information lower BOund (CMES-IBO), that is based on a Monte Carlo (MC) estimator of a lower bound of a mutual information (MI). We first define the MI in which the max-value is defined so that it can incorporate uncertainty with respect to feasibility. Then, we derive a lower bound of the MI that guarantees non-negativity, while a constrained counterpart of conventional MES can be negative. We further provide theoretical analysis that assures the low-variability of our estimator which has never been investigated for any existing information-theoretic BO. Moreover, using the conditional MI, we extend CMES-IBO to the parallel setting while maintaining the desirable properties. We demonstrate the effectiveness of CMES-IBO by several benchmark functions and a real-world problem.

1 Introduction

Bayesian optimization (BO) has been widely studied as an effective framework for expensive black-box optimization problems. On the other hand, various real-world problems have additional unknown *constraints*. For example, materials discovery can be seen as an optimization of a physical property of materials, such as conductivity, under constraints derived from other physical properties, such as stability. However, this task is often quite difficult because in many practical problems, measuring these properties comes at a high cost, and further, functional forms of both objective and constraint properties are unknown (black-box functions).

To incorporate unknown constraint functions, *constrained BO* (CBO) has also been studied [Gardner et al., 2014, Gelbart et al., 2014, Schonlau et al., 1998, Snoek, 2013]. CBO tries to achieve the sample-efficient optimization by repeatedly observing objective and constraint functions that are estimated to be beneficial to identify the optimal solution.

Max-value entropy search (MES) [Wang and Jegelka, 2017] is one of the state-of-the-art approaches in BO. The basic idea is to maximize the mutual information (MI) between a querying point and the optimal objective value. For constrained problems, Perrone et al. [2019] have proposed an extension of MES, but it is restricted to only one constraint (note that although their main focus is on a setting in which only a binary indicator of feasibility is observed for constraints, they also show the ‘real-valued feedback’ case in the appendix). Although it is possible to consider a multiple constraint extension of this approach, which we call constrained MES (CMES), the resulting MI approximation can have a negative value (though the MI should be non-negative) when the number of constraints is more than 5 as we will show in Section 4.1. A more comprehensive review of related studies is shown in Section 5.

In this paper, we propose a novel information-theoretic CBO method called *Constrained Max-value Entropy Search via Information lower BOund* (CMES-IBO), which is based on a Monte Carlo (MC) estimator of a lower bound of an MI. We first define the MI in which the random max-value is defined so that it can incorporate uncertainty with respect to feasibility (whether the problem has a feasible region or not). This issue has not been considered by existing information-theoretic CBO studies, though for constrained problems in general, to identify the feasibility of the problem is a key issue (called the feasibility problem [Chinneck, 2007]). Then, we derive an acquisition function based on a lower bound of the MI that can guarantee non-negativity. We empirically observe that CMES-IBO can provide reasonable acquisition function values even when CMES provides negative values. Further, we provide theoretical analysis that assures the low-variability of our estimator, such as a concentration bound achieving an exponentially fast convergence to the true lower bound in the number of MC samples, which has never been investigated for any existing information-theoretic BO. Moreover, using the conditional MI, we extend CMES-IBO to the parallel setting while maintaining the desirable properties.

Our main contributions are summarized as follows:

1. We develop an MI lower bound based CBO called CMES-IBO. Our MI is well-defined even when a feasible region can be empty, and the resulting MI approximation becomes quite simple and guarantees non-negativity.
2. We consider differences of CMES-IBO from the more direct MES extension, called CMES, that has the possible negativity issue, and we also provide analysis on the estimation variability of our estimator.
3. We further develop a parallel extension of CMES-IBO, in which multiple queries can be issued simultaneously. The extension is based on a combination of the conditional MI and the greedy selection.

We demonstrate the effectiveness of CMES-IBO by benchmark and real-world functions.

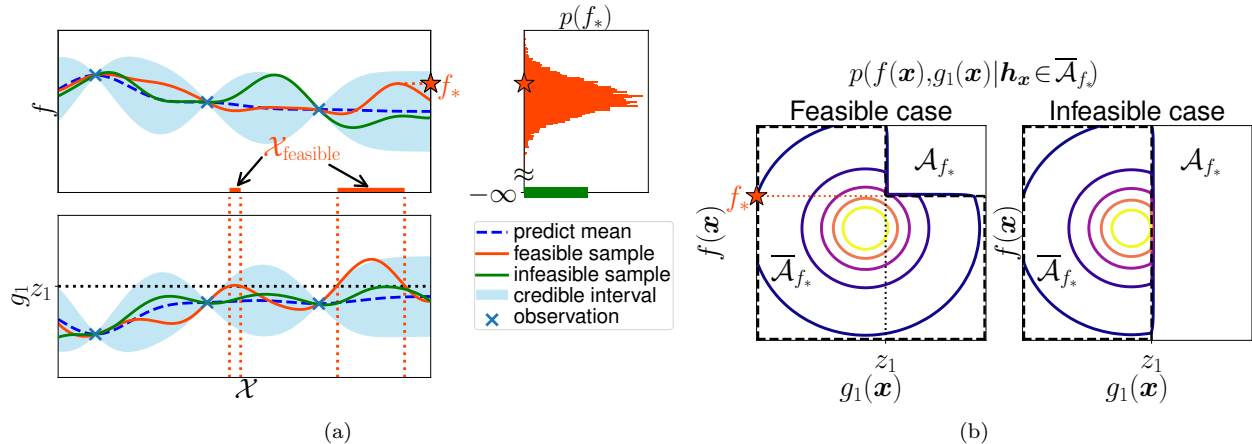


Figure 1: Generative process of the optimal value f_* and truncation of the predictive distribution. (a) In the left two plots, two sets of sample paths (red and green) are generated from GPs. The red sample path of g_1 has the non-empty feasible region $\mathcal{X}_{\text{feasible}}$ while the green sample path has an empty feasible region. The red star is the optimal value of the red sample path, and for the green sample path, the optimal value is defined as $-\infty$ as shown in (1). The distribution of the optimal value is plotted in the upper right figure. (b) The two contour plots represent the density function $p(\mathbf{h}_{\mathbf{x}} | \mathbf{h}_{\mathbf{x}} \in \bar{\mathcal{A}}_{f_*}) = p(f(\mathbf{x}), g_1(\mathbf{x}) | \mathbf{h}_{\mathbf{x}} \in \bar{\mathcal{A}}_{f_*})$ for the feasible and infeasible cases, respectively. For a given f_* , the density should be 0 in \mathcal{A}_{f_*} , because $f(\mathbf{x})$ cannot be larger than the given f_* for \mathbf{x} such that $g_1(\mathbf{x}) \geq z_1$.

2 Preliminary

We are interested in the maximum value of the objective function $f : \mathcal{X} \mapsto \mathbb{R}$ under C constraint functions $g_c : \mathcal{X} \mapsto \mathbb{R}$ for $c = 1, \dots, C$, where $\mathcal{X} \subset \mathbb{R}^d$ is an input space. Let $\mathcal{X}_{\text{feasible}} := \{\mathbf{x} \mid g_c(\mathbf{x}) \geq z_c, c = 1, \dots, C\}$ be the feasible region, where $z_c \in \mathbb{R}$ is a given constant. The optimal solution of this constrained optimization problem is written as $\mathbf{x}_* := \arg \max_{\mathbf{x} \in \mathcal{X}_{\text{feasible}}} f(\mathbf{x})$. We consider the setting that the functions f and g_1, \dots, g_C are unknown but can be evaluated simultaneously for any given $\mathbf{x} \in \mathcal{X}$ with high observation cost. We assume that f and g_1, \dots, g_C follow independent *Gaussian processes* (GPs). Suppose that we already queried n points $\{(f(\mathbf{x}_i), g_1(\mathbf{x}_i), \dots, g_C(\mathbf{x}_i))\}_{i=1, \dots, n}$ for each of $f(\mathbf{x}_i)$ and $g_c(\mathbf{x}_i)$, actual observations can be contaminated with additive noises generated by a Gaussian distribution. We write predictive distributions of $f(\mathbf{x})$ and $g_c(\mathbf{x})$ as $\mathcal{N}(\mu_n^{(f)}(\mathbf{x}), \sigma_n^{(f)2}(\mathbf{x}))$ and $\mathcal{N}(\mu_n^{(g_c)}(\mathbf{x}), \sigma_n^{(g_c)2}(\mathbf{x}))$, respectively. Since we use standard GP models, detailed definitions of these posteriors are omitted here (see Appendix A).

3 Constrained Max-value Entropy Search via Information Lower Bound

3.1 Max-value of Constrained Problem

First, we consider the definition of a random variable f_* , which is the max-value of a constraint optimization problem. The straightforward definition is $\max_{\mathbf{x} \in \mathcal{X}_{\text{feasible}}} f(\mathbf{x})$, employed in a prior work on the MES-based CBO [Perrone et al., 2019]. However, this definition is not well-defined as a proper random variable when $\mathcal{X}_{\text{feasible}}$ can be empty, i.e., when $\Pr(\mathcal{X}_{\text{feasible}} = \emptyset) > 0$. Note that $\mathcal{X}_{\text{feasible}}$ is randomly determined through GPs g_1, \dots, g_C , and thus, $\Pr(\mathcal{X}_{\text{feasible}} = \emptyset) > 0$ can occur even when the underlying unknown true constraint functions have a non-empty feasible region. Thus, we define f_* as follows:

$$f_* := \begin{cases} \max_{\mathbf{x} \in \mathcal{X}_{\text{feasible}}} f(\mathbf{x}), & \text{if } \mathcal{X}_{\text{feasible}} \neq \emptyset, \\ -\infty, & \text{otherwise.} \end{cases} \quad (1)$$

Regarding the optimal value as $-\infty$ when no feasible solution exists is a common convention in classical optimization literature [Boyd and Vandenberghe, 2004]. The schematic illustration of f_* is shown in Figure 1 (a). Note that $p(f_*)$ can be seen as a mixture distribution of the discrete and continuous variables (red and green histograms in the figure). The figure indicates that our definition of $p(f_*)$ can incorporate the uncertainty about whether the problem is feasible or not.

3.2 Acquisition Function of CMES-IBO

Let

$$\mathbf{h}_{\mathbf{x}} := (f(\mathbf{x}), g_1(\mathbf{x}), \dots, g_C(\mathbf{x}))^\top \in \mathbb{R}^{C+1},$$

be a vector concatenating the objective and all the constraint functions. Suppose that we already have the dataset \mathcal{D}_{t-1} , which contains observations for the past $t-1$ queries. We consider selecting a next query \mathbf{x}_t by maximizing the MI between $\mathbf{h}_{\mathbf{x}}$ and f_* given \mathcal{D}_{t-1} :

$$\text{MI}(\mathbf{h}_{\mathbf{x}}; f_* | \mathcal{D}_{t-1}). \quad (2)$$

Hereafter, we omit the conditioning by \mathcal{D}_{t-1} in MI, entropy, density, and probability when it is obvious from the context. For example, $p(\mathbf{h}_{\mathbf{x}} | f_*)$ indicates $p(\mathbf{h}_{\mathbf{x}} | \mathcal{D}_{t-1}, f_*)$.

Since directly evaluating the MI (2) is computationally intractable, we consider a lower bound derived as follows:

$$\begin{aligned} \text{MI}(\mathbf{h}_{\mathbf{x}}; f_*) &= \mathbb{E}_{f_*} \left[\int p(\mathbf{h}_{\mathbf{x}} | f_*) \log \frac{p(\mathbf{h}_{\mathbf{x}} | f_*)}{p(\mathbf{h}_{\mathbf{x}})} d\mathbf{h}_{\mathbf{x}} \right] \\ &= \mathbb{E}_{f_*} \left[\int p(\mathbf{h}_{\mathbf{x}} | f_*) \log \frac{q(\mathbf{h}_{\mathbf{x}})}{p(\mathbf{h}_{\mathbf{x}})} d\mathbf{h}_{\mathbf{x}} + D_{\text{KL}}(p(\mathbf{h}_{\mathbf{x}} | f_*) || q(\mathbf{h}_{\mathbf{x}})) \right] \\ &\geq \mathbb{E}_{f_*} \left[\int p(\mathbf{h}_{\mathbf{x}} | f_*) \log \frac{q(\mathbf{h}_{\mathbf{x}})}{p(\mathbf{h}_{\mathbf{x}})} d\mathbf{h}_{\mathbf{x}} \right], \end{aligned} \quad (3)$$

where $D_{\text{KL}}(\cdot)$ is Kullback-Leibler (KL) divergence and $q(\mathbf{h}_{\mathbf{x}})$ is an arbitrary probability density function (PDF) that has same support as $p(\mathbf{h}_{\mathbf{x}}|f_*)$. See Appendix B for the derivation. The difference between the lower bound and the MI is given as $\mathbb{E}_{f_*}[D_{\text{KL}}(p(\mathbf{h}_{\mathbf{x}}|f_*)||q(\mathbf{h}_{\mathbf{x}}))]$, and thus, the equality holds if $p(\mathbf{h}_{\mathbf{x}}|f_*)$ is equal to $q(\mathbf{h}_{\mathbf{x}})$ for $\forall f_*$.

To use the lower bound (3), we have to specify the distribution $q(\mathbf{h}_{\mathbf{x}})$. For this type of KL-based lower bounds, the variational approximation is a well-known approach by which the lower bound is maximized with respect to $q(\mathbf{h}_{\mathbf{x}})$. However, the expectation and the integral with respect to f_* and $\mathbf{h}_{\mathbf{x}}$ in (3) make this optimization computationally too complicated. Instead, we consider setting $q(\mathbf{h}_{\mathbf{x}})$ as a specific distribution that can be easily computed.

The optimal selection of $q(\mathbf{h}_{\mathbf{x}})$ is $p(\mathbf{h}_{\mathbf{x}}|f_*)$, i.e., predictive distributions of GPs given the optimal value f_* which we call a $\text{GP}|_{f_*}$. For all existing MES-based approaches, the $\text{GP}|_{f_*}$ is required in a slightly different context (see Section 4.1 for the case of the existing MES for constrained problems). Since the $\text{GP}|_{f_*}$ is difficult to evaluate, it is approximated by a distribution defined by truncating the original GP predictive distribution at f_* in almost all the existing methods [e.g., Wang and Jegelka, 2017, Takeno et al., 2020, Perrone et al., 2019, Suzuki et al., 2020]. For example, in the case of the original MES, $p(f(\mathbf{x}) | f_*)$ is replaced with $p(f(\mathbf{x}) | f(\mathbf{x}) \leq f_*)$, which is the normal distribution truncated at f_* . This replacement makes the resulting acquisition function simple and practical performance of MES-based approaches with this replacement has been repeatedly shown. Therefore, we follow this truncation-based approach.

In the case of constrained problems, when the optimal value f_* is fixed, $f(\mathbf{x}) > f_*$ does not hold if $g_c(\mathbf{x}) \geq z_c$ for $\forall c$ (i.e., \mathbf{x} is feasible). This means that $f(\mathbf{x})$ and $g_c(\mathbf{x})$ are jointly truncated so that their densities become 0 in $\mathcal{A}_{f_*} := (f_*, \infty) \times (z_1, \infty) \times \dots \times (z_C, \infty) \subset \mathbb{R}^{C+1}$. In other words, $\mathbf{h}_{\mathbf{x}}$ should be in $\bar{\mathcal{A}}_{f_*} \subset \mathbb{R}^{C+1}$, which is a complementary set of \mathcal{A}_{f_*} , as illustrated in Figure 1 (b). Thus, we set $q(\mathbf{h}_{\mathbf{x}})$ as the following *truncated multivariate normal* (TMN) distribution:

$$\begin{aligned} q(\mathbf{h}_{\mathbf{x}}) &= p(\mathbf{h}_{\mathbf{x}} | \mathbf{h}_{\mathbf{x}} \in \bar{\mathcal{A}}_{f_*}) \\ &= \begin{cases} p(\mathbf{h}_{\mathbf{x}})/\bar{Z}_{\mathbf{x}}(f_*) & \text{for } \mathbf{h}_{\mathbf{x}} \in \bar{\mathcal{A}}_{f_*}, \\ 0 & \text{for } \mathbf{h}_{\mathbf{x}} \in \mathcal{A}_{f_*}, \end{cases} \end{aligned} \quad (4)$$

where the normalization constant $\bar{Z}_{\mathbf{x}}(f_*) = \Pr(\mathbf{h}_{\mathbf{x}} \in \bar{\mathcal{A}}_{f_*})$.

For any given f_* , the normalization constant $\bar{Z}_{\mathbf{x}}(f_*)$ can be computed easily. Let $Z_{\mathbf{x}}(f_*) := \Pr(\mathbf{h}_{\mathbf{x}} \in \mathcal{A}_{f_*})$, and then, $\bar{Z}_{\mathbf{x}}(f_*) = 1 - Z_{\mathbf{x}}(f_*)$. Since \mathcal{A}_{f_*} is a hyperrectangle, based on the independence assumption of f and g_c for $\forall c$, we can decompose $Z_{\mathbf{x}}(f_*)$ as follows:

$$\begin{aligned} Z_{\mathbf{x}}(f_*) &= \Pr(f(\mathbf{x}) \geq f_*) \prod_{c=1}^C \Pr(g(\mathbf{x}) \geq z_c) \\ &= (1 - \Phi(\gamma_t^{(f)}(\mathbf{x}))) \prod_{c=1}^C (1 - \Phi(\gamma_t^{(g_c)}(\mathbf{x}))), \end{aligned} \quad (5)$$

where $\gamma_t^{(f)}(\mathbf{x}) := (f_* - \mu_{t-1}^{(f)}(\mathbf{x}))/\sigma_{t-1}^{(f)}(\mathbf{x})$, $\gamma_t^{(g_c)}(\mathbf{x}) := (z_c - \mu_{t-1}^{(g_c)}(\mathbf{x}))/\sigma_{t-1}^{(g_c)}(\mathbf{x})$, and Φ is the cumulative distribution function (CDF) of the standard normal distribution.

By substituting TMN (4) and $\bar{Z}_{\mathbf{x}}(f_*) = 1 - Z_{\mathbf{x}}(f_*)$ into (3), we obtain a lower bound $L(\mathbf{x})$ as

$$\begin{aligned} L(\mathbf{x}) &:= \mathbb{E}_{f_*} \left[\int_{\mathcal{A}_{f_*}} p(\mathbf{h}_{\mathbf{x}}|f_*) \log \frac{p(\mathbf{h}_{\mathbf{x}})/(1 - Z_{\mathbf{x}}(f_*))}{p(\mathbf{h}_{\mathbf{x}})} d\mathbf{h}_{\mathbf{x}} \right] \\ &= \mathbb{E}_{f_*} [-\log(1 - Z_{\mathbf{x}}(f_*))]. \end{aligned} \quad (6)$$

See Appendix B for the detailed derivation. In (6), $C + 1$ dimensional integral with respect to $\mathbf{h}_{\mathbf{x}}$ is canceled out, which is one of important benefits of our selection of $q(\mathbf{h}_{\mathbf{x}})$. By applying the MC approximation to \mathbb{E}_{f_*} in (6), we obtain the CMES-IBO acquisition function

$$\alpha_t^{\text{IBO}}(\mathbf{x}) = -\frac{1}{K} \sum_{f_* \in \mathcal{F}_*} \log(1 - Z_{\mathbf{x}}(f_*)), \quad (7)$$

where \mathcal{F}_* is a set of the sampled f_* from the current GPs and $K = |\mathcal{F}_*|$. Consequently, our acquisition function is reduced to a simple functional form.

The algorithm for our CMES-IBO is shown in Appendix H. Although we mainly focus on the setting that GPs are independent of each other, CMES-IBO can also apply to the correlated setting easily by computing $Z_{\mathbf{x}}(f_*) = \Pr(\mathbf{h}_{\mathbf{x}} \in \mathcal{A}_{f_*})$ as the CDF of the multivariate (correlated) normal distribution.

3.3 Sampling f_*

When \mathcal{X} is a finite set of a moderate size, f_* can be sampled from the joint predictive distributions of $\mathbf{h}_{\mathbf{x}}$ for all candidate points $\mathbf{x} \in \mathcal{X}$. Otherwise (such as a continuous \mathcal{X}), we employ an approach using the random Fourier feature (RFF) [Rahimi and Recht, 2008]. We first generate approximate sample paths of objective and constraint functions from Bayesian linear regression models using RFF, and then, we solve a (white-box) constrained optimization problem defined by the generated sample paths by using a general solver (see Appendix H.1 for details). A similar approach has been commonly employed in the entropy-based BO [e.g., Wang and Jegelka, 2017]. Particularly when the dataset \mathcal{D}_{t-1} does not contain any feasible solution (which typically occurs at the beginning of the optimization), sampled $\mathcal{X}_{\text{feasible}}$ is often empty, as shown in the green sample path in Figure 1 (b). Therefore, if the solver cannot find any feasible solution, f_* is set as $-\infty$ as defined in (1).

3.4 Parallelization

We consider a parallel extension, in which Q queries can be evaluated at every iteration. Due to a space limitation, we here only describe the main idea briefly (see Appendix C for more detail). We employ a greedy selection of the Q queries using the *conditional mutual information* (CMI). Let $\mathcal{X}_q := \{\mathbf{x}^{(1)}, \dots, \mathbf{x}^{(q)}\}$ and $\mathcal{H}_q := \{\mathbf{h}_{\mathbf{x}^{(1)}}, \dots, \mathbf{h}_{\mathbf{x}^{(q)}}\}$ be sets of q inputs and output vectors already selected in the greedy procedure ($q < Q$), respectively. To maximize the MI after adding the $(q + 1)$ -th query \mathbf{x} , i.e., $\text{MI}(\mathcal{H}_q \cup \mathbf{h}_{\mathbf{x}}; f_*)$, we consider the decomposition

$$\text{MI}(\mathcal{H}_q \cup \mathbf{h}_{\mathbf{x}}; f_*) = \text{MI}(\mathcal{H}_q; f_*) + \text{CMI}(\mathbf{h}_{\mathbf{x}}; f_* | \mathcal{H}_q),$$

where $\text{CMI}(\mathbf{h}_x; f_* | \mathcal{H}_q) := \mathbb{E}_{\mathcal{H}_q} [\text{MI}(\mathbf{h}_x; f_* | \mathcal{H}_q)]$. Since the first term does not depend on \mathbf{x} , we only need to maximize $\text{CMI}(\mathbf{h}_x; f_* | \mathcal{H}_q)$.

By the same approach as (6), we can obtain the lower bound of $\text{CMI}(\mathbf{h}_x; f_* | \mathcal{H}_q)$ as

$$L(\mathbf{x} | \mathcal{X}_q) := -\mathbb{E}_{\mathcal{H}_q, f_*} [\log(1 - Z_{\mathbf{x}}(f_* | \mathcal{H}_q))], \quad (8)$$

where $Z_{\mathbf{x}}(f_* | \mathcal{H}_q) := \Pr(\mathbf{h}_x \in \mathcal{A}_{f_*} | \mathcal{X}_q, \mathcal{H}_q)$. See Appendix B for the derivation. Given $\mathcal{X}_q, \mathcal{H}_q$ and f_* , $Z_{\mathbf{x}}(f_* | \mathcal{H}_q)$ can be easily computed through the GPs updated by \mathcal{X}_q and \mathcal{H}_q . By applying the MC estimation, we obtain the acquisition function for the $(q+1)$ -th query as

$$\alpha_t^{\text{IBO}}(\mathbf{x} | \mathcal{X}_q) = -\frac{1}{K} \sum_{(f_*, \mathcal{H}_q) \in \mathcal{J}} \log(1 - Z_{\mathbf{x}}(f_* | \mathcal{H}_q)), \quad (9)$$

where \mathcal{J} is a set of K sampled (f_*, \mathcal{H}_q) from the current GPs. Note that jointly sampling f_* and \mathcal{H}_q can be easily performed by almost the same procedure as the sequential case (see Appendix H.1 for detail). Consequently, our parallel extension is also reduced to a simple acquisition function.

4 Analysis

We here consider differences of CMES-IBO from a more direct application of the conventional MES, and we also provide analysis on the estimation variability of our estimator. Although we focus on the sequential case, both of them also hold in the parallel case.

4.1 Comparison with Conventional MES

Although we employ the lower bound based approach to derive CMES-IBO, Perrone et al. [2019] have proposed a more direct extension of MES to CBO (Note that Perrone et al. [2019] mainly focus on the binary setting, in which a binary value indicating feasible or not is only observed). However, their derivation is restricted to only one constraint ($C = 1$). Although Fernández-Sánchez et al. [2020] described that the extension to multiple constraints is not obvious, to consider the relation with CMES-IBO, we extend this original MES-based approach to the multiple constraints case, which we refer to as CMES.

In CMES, the MI is approximated as

$$\begin{aligned} \text{MI}(\mathbf{h}_x; f_*) &= H(\mathbf{h}_x) - \mathbb{E}_{f_*} [H(\mathbf{h}_x | f_*)] \\ &\approx H(\mathbf{h}_x) - \mathbb{E}_{f_*} [H(\mathbf{h}_x | \mathbf{h}_x \in \bar{\mathcal{A}}_{f_*})] \end{aligned} \quad (10)$$

$$\begin{aligned} &\approx \frac{1}{K} \sum_{f_* \in \mathcal{F}_*} \left\{ \frac{Z_{\mathbf{x}}(f_*)}{2(1 - Z_{\mathbf{x}}(f_*))} R_{f_*} - \log(1 - Z_{\mathbf{x}}(f_*)) \right\} \\ &=: \alpha_t^{\text{CMES}}(\mathbf{x}), \end{aligned} \quad (11)$$

where

$$R_{f_*} = \frac{\gamma_t^{(f)}(\mathbf{x}) \phi(\gamma_t^{(f)}(\mathbf{x}))}{1 - \Phi(\gamma_t^{(f)}(\mathbf{x}))} + \sum_{c=1}^C \frac{\gamma_t^{(g_c)}(\mathbf{x}) \phi(\gamma_t^{(g_c)}(\mathbf{x}))}{1 - \Phi(\gamma_t^{(g_c)}(\mathbf{x}))},$$

and $H(\cdot)$ is the differential entropy and ϕ is the PDF of the standard normal distribution. See Appendix F for the derivation. The first approximation (10) is the replacement from $p(\mathbf{h}_x | f_*)$ to $p(\mathbf{h}_x | \mathbf{h}_x \in \bar{\mathcal{A}}_{f_*})$ in the entropy of the second term, and the second approximation that derives the next line is the MC estimation of \mathbb{E}_{f_*} (Note that although the approximation strategy follows [Perrone et al., 2019], f_* here is based on our definition (1) because f_* should be a proper random variable to define the MI as we mentioned in Section 3.1).

Although CMES can be seen as a constrained counterpart of the original MES, the following lemma reveals that the MI approximation of CMES (11) can be a negative value when $C > 5$.

Lemma 4.1. *When $C > 5$, for every $t \geq 1$ and $\mathbf{x} \in \mathcal{X}$, there exist thresholds $z_c (c = 1, \dots, C)$ that result in $\Pr(\alpha_t^{\text{CMES}}(\mathbf{x}) < 0) > 0$*

See Appendix F.3 for the proof. In contrast, for CMES-IBO, we have the following remark:

Remarks 4.1. *Our acquisition function is bounded from below by an average of probability of improvement (PI) from f_* , i.e., $\alpha_t^{\text{IBO}}(\mathbf{x}) \geq \sum_{f_* \in \mathcal{F}_*} \Pr(\mathbf{h}_x \in \mathcal{A}_{f_*})/K \geq 0$, from which we also see non-negativity.*

This remark is immediately derived by applying the well-known inequality $\log x \leq x - 1$ to (7). Note that $\Pr(\mathbf{h}_x \in \mathcal{A}_{f_*})$ is PI from f_* because it is the probability that $f(\mathbf{x}) \geq f_*$ and $g_c(\mathbf{x}) \geq z_c$ for $\forall c$. The (unconstrained) MES also has shown a relation with PI [Wang and Jegelka, 2017], while for CMES, it is difficult to see a clear relation with PI. Let the worst-case error be the largest error of the MI approximation among all the possible optimal-value samples \mathcal{F}_* . For problems in which $\Pr(\alpha_t^{\text{CMES}}(\mathbf{x}) < 0) > 0$, the worst-case error of CMES-IBO is smaller than that of CMES.

The negative value of CMES is not only a theoretical possibility. Figure 2 shows an example in a toy problem. We assume that all constraints g_1, \dots, g_C are the same function just for simplicity and change C from 4 to 7. CMES and CMES-IBO are calculated with $K = 10$. In the figure, we also provide a numerical approximation of the original MI naïvely estimated by using the kernel density estimation (KDE), denoted as KDE-MI. For KDE-MI, we use a large number of samples (10000), which cannot be performed in practice. To demonstrate negativity of CMES, the threshold z_c (shown in Figure 2 (b)) is set so that R_{f_*} in CMES (11) becomes large negative value around $x = 0.9$ particularly when C is large. Then, in fact, CMES takes negative values around the global optima of KDE-MI in the case of $C = 6$ and 7. On the other hand, CMES-IBO keeps the same global optima as KDE-MI among 200 grid points for all C . Although CMES has a negative value only when $C > 5$ as Lemma 4.1 indicates, the acquisition values gradually decrease with the growth of C . Although values of CMES-IBO are nearly half of KDE-MI, we can clearly see they are highly correlated. Further detail of this example is in Appendix F.4.

Note that, in practice, the problematic behavior of CMES shown in Figure 2 (c) does not occur frequently depending on the given problem setting. Although we will see that CMES often reasonably works in later experiments, the potential risk of this negativity issue degrades reliability of CMES.

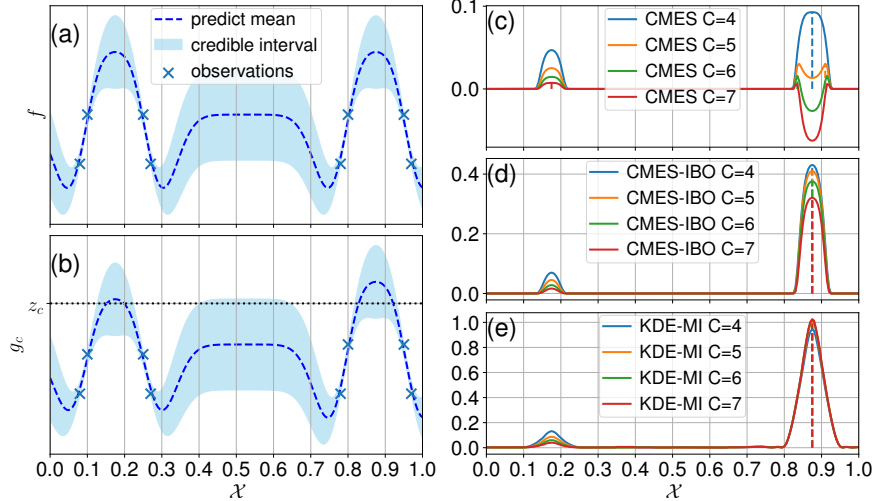


Figure 2: In (a) and (b), the GPs for f and g_c are shown, respectively. In (c)-(e), CMES, CMES-IBO, and the KDE-based MI approximation are shown, and each vertical dotted line indicates the maximum.

4.2 Bounds for Estimation Variability

We here analyze variability of our MI estimator (7), that is, how the MI estimator (7) deviates from its expectation (6). The simplicity of our MI estimator (7) enables us to derive the following theorem, while it is difficult to derive a similar guarantee for CMES:

Theorem 4.1. *For every $t \geq 1$ and $\mathbf{x} \in \mathcal{X}$, our MI estimator (7) satisfies $\mathbb{V}_{f_*}[-\log(1 - Z_{\mathbf{x}}(f_*))] \leq 2$, where \mathbb{V}_{f_*} represents the variance with respect to f_* . Moreover, for every $\xi \geq 0$, $t \geq 1$ and $\mathbf{x} \in \mathcal{X}$, following concentration inequality holds*

$$\Pr\{|\alpha_t^{IBO}(\mathbf{x}) - L(\mathbf{x})| \geq \xi\} \leq \min\{U_1, U_2\}, \quad (12)$$

where $U_1 = \frac{2}{K\xi^2}$ and $U_2 = 2 \exp\left[-AK \min\left(\frac{\xi^2}{B^2}, \frac{\xi}{B}\right)\right]$ with constants A and B .

See Appendix D for the proof.

The variance of our MI estimator with $K = 1$ can be bounded by the constant 2, and this fact provides the bound by U_1 as a direct consequence of Chebyshev's inequality. Most importantly, U_2 yields exponentially fast decay on K and ξ in contrast to the linear and quadratic dependence by U_1 . Although the convergence rate of U_1 is worse than U_2 , U_1 may provide a tighter bound for specific values of K and ξ . Note that our bound (12) holds for any number of samplings K , i.e., it is not an asymptotic result such as the central limit theorem. Moreover, U_1 and U_2 do not depend on any parameter of GPs and the problem setting, such as $\sigma_{t-1}^{(f)2}(\mathbf{x})$, $\sigma_{t-1}^{(g_c)2}(\mathbf{x})$, and C . Our analysis can be seen as a guarantee of the estimation robustness of CMES-IBO even with a small K .

5 Related Work

Extensions of unconstrained BO methods to CBO have been widely studied. The standard expected improvement (EI) based approaches are called *EI with Constraint* (EIC) [Schonlau et al., 1998, Snoek, 2013, Gelbart et al., 2014, Gardner et al., 2014]. However, when no feasible solution is obtained, the so-called ‘current best solution’ can not be defined. To avoid this difficulty, heuristic strategies, such as only using the feasible probability [Gelbart et al., 2014] and introducing a threshold hyperparameter [Letham et al., 2019], have been considered, but an appropriate remedy for this issue is still an open problem. Gramacy and Lee [2010] and Picheny [2014] consider the expected reduction of EI and PI, respectively. However, since these approaches require expensive numerical integrations defined on the entire domain \mathcal{X} , their applicability is limited. A *Thompson Sampling* (TS) based method called *Scalable Constrained BO* (SCBO) [Eriksson and Poloczek, 2021] has been proposed, recently. The standard TS is justified by strong theoretical results [Kandasamy et al., 2018], but the convergence rate for the regret of SCBO has not been shown.

The augmented Lagrangian (AL), which is a classical approach to white-box constrained problems, has also been combined with BO [Gramacy et al., 2016, Picheny et al., 2016]. In AL-based methods, initial parameters of a Lagrange multiplier and a penalty coefficient should be specified. In the classical white-box optimization, these parameters can be refined during a large number of iterations. However, for expensive black-box problems, the number of possible iterations is much smaller than the classical optimization, and the effect of the initial parameters can be significant. Ariaifar et al. [2019] proposed *Alternating Direction Method of Multipliers BO* (ADMMBO) based on the famous ADMM algorithm. ADMMBO is only for decoupled setting, in which each one of objective and constraint functions is observed separately. In this paper, we only focus on the setting in which objective and constraint functions are simultaneously observed.

Entropy-based approaches are also studied in CBO literature. Hernández-Lobato et al. [2015, 2016] proposed *Predictive Entropy Search with Constraint* (PESC), which is an extension of a prior work on unconstrained problems [Hernández-Lobato et al., 2014]. PESC considers the information gain of the optimal \mathbf{x}_* , but complicated approximations, for which any relation with the original MI has not been clarified, are required. Another well-known entropy-based BO is MES, for which we already discussed in Section 4.1. MES for multi-objective problems with constraints has been recently proposed by two papers [Belakaria et al., 2020, Fernández-Sánchez et al., 2020]. Fernández-Sánchez et al. [2020] pointed out that the entropy evaluation of [Belakaria et al., 2020] is incorrect and derived a multi-objective counterpart of CMES (10), but they introduced multiple additional approximations by which the relation with the original MI is further unclear. Moreover, it is worth noting that none of the information-theoretic CBO studies have considered the possibility of $\mathcal{X}_{\text{feasible}} = \emptyset$. See Appendix E for a detailed discussion on this problem.

A simple approach to incorporating multiple constraints is to transform it into a single constraint such as $g(\mathbf{x}) := \min_c(g_c(\mathbf{x}) - z_c) \geq 0$. Both of fitting a GP directly to $g(\mathbf{x})$ and fitting GPs to $g_c(\mathbf{x})$ individually are possible strategies in this case, but the former discards observations of each $g_c(\mathbf{x})$ (only use the min value) and the later makes $g(\mathbf{x})$ non-Gaussian. The binary setting approach [Perrone et al., 2019] can also be used

for this purpose, but then, observations of each $g_c(\mathbf{x})$ are discarded.

The parallel extension of CBO has not been widely studied. Letham et al. [2019] have shown the parallel CBO based on EIC. Although Eriksson and Poloczek [2021] have not focused on the parallelization, SCBO is applicable to the parallel setting easily because of the nature of TS. For MES, although [Takeno et al., 2020] have proposed a CMI based parallel BO for the multi-fidelity setting, their approach is not based on a lower bound of CMI, and constrained problems have not been studied. Wilson et al. [2018] discussed the MC-based parallel BO in general, but they considered only ‘myopic maximal (MM) acquisition functions.’ MES is not included in the class of MM acquisition functions, and CBO was not considered in Wilson et al. [2018].

To our knowledge, no existing studies use a lower bound of the MI for BO. Moss et al. [2021] recently proposed a lower bound based extension of MES. However, their bound is a lower bound of the ‘approximate’ MI used in the original MES, which is not a lower bound of the MI, and constrained problems have not been studied. Although we only focus on constrained problems, considering the effectiveness of the lower bound approach to the unconstrained problem is one of our important future works.

Lastly, we mention regret analysis of the entropy-based BO. Wang and Jegelka [2017] show the regret analysis of ‘one sample MES,’ in which only one optimal value is sampled in the MC estimation. To our knowledge, no other regret analysis is known for the entropy-based BO (Belakaria et al. [2019] shows an extension to the multi-objective problem, but their regret can be negative value as pointed out by Suzuki et al. [2020]). However, the original theorem of MES contains several technical problems. For example, the theorem assumes that f follows a GP, but the maximum of f is regarded as a deterministic variable in the proof, which contradicts each other (more details including other issues are in Appendix I). Therefore, convergence guarantee is still an open problem for the entropy-based BO.

6 Experiments

We demonstrate the performance of sequential optimization by comparing with CMES, EIC [Gelbart et al., 2014], a TS-based method referred to as TSC, and PESC [Hernández-Lobato et al., 2015] in Spearmint (<https://github.com/HIPS/Spearmint/tree/PESC>). Note that CMES is based on our definition of f_* (1). TSC is a variant of SCBO [Eriksson and Poloczek, 2021] simplified by omitting the output transformation (such as the Gaussian copula-based transformation of the objective) and the trust region strategy. Since these two are general strategies applicable to any acquisition functions, to only focus on the difference of acquisition functions, we do not employ them. Although the AL-based methods [Gramacy et al., 2016, Picheny et al., 2016] are not shown as baselines, they are outperformed by PESC and SCBO in prior work [Hernández-Lobato et al., 2015, Eriksson and Poloczek, 2021], respectively.

Performances on GP-derived synthetic functions, benchmark functions, and a real-world problem were evaluated by using the *utility gap*, which is also employed in various prior work [Hernández-Lobato et al.,

2015, Picheny et al., 2016, Eriksson and Poloczek, 2021]. We set the recommendation at iteration t as $\hat{\mathbf{x}}_t = \arg \max_{\mathbf{x} \in \mathcal{X}} \mu_{t-1}^{(f)}(\mathbf{x})$, s.t. $\forall c, \Pr(g_c(\mathbf{x}) \geq z_c) \geq \sqrt[3]{0.95}$. Then, the utility gap is defined as $f_* - f(\hat{\mathbf{x}}_t)$ if the recommendation is feasible, otherwise $f_* - \min_{\mathbf{x} \in \mathcal{X}} f(\mathbf{x})$, which indicates that an infeasible recommendation results in the worst utility gap. The initial inputs are sampled by Latin hypercube sampling [Loh, 1996]. The sample size of all MC approximations is set as 10. For the kernel function in GPs, we used a linear combination of the linear kernel $k_{\text{LIN}} : \mathcal{X} \times \mathcal{X} \rightarrow \mathbb{R}$ and RBF kernel $k_{\text{RBF}} : \mathcal{X} \times \mathcal{X} \rightarrow \mathbb{R}$ defined as $\sigma_{\text{LIN}}^2 k_{\text{LIN}}(\mathbf{x}, \mathbf{x}') + \sigma_{\text{RBF}}^2 k_{\text{RBF}}(\mathbf{x}, \mathbf{x}')$, where σ_{LIN}^2 and σ_{RBF}^2 are updated by the marginal likelihood maximization every 5 iteration, except for the GP-derived functions in which all the methods employed the same fixed kernels used to generate the true functions. We used k_{LIN} because our benchmark functions often contain linear functions. For the GP-derived functions, we generated 10 constrained problems for each of which the experiment is run 10 times, and the mean and standard error of the total 100 trials are reported. For benchmark and the real-word function, we report the mean and the standard error of 10 random initializations. For PESC, due to difficulty rewriting the Spearmint specification, the default settings of kernels and inner optimization are used. Although PESC has the same number of initial points, their location is not identical to other methods because of the same reason. Other experimental details such as the number of initial points are shown in Appendix J.

First, we focus on the results for the sequential querying shown in Figure 3.

GP-derived synthetic functions (a): The objective and the $C = 10$ constraints are sampled from zero-mean GPs with RBF kernels whose length scales are 0.2. The thresholds are set as $z_c = -0.75$ for $\forall c$, and the input domain is $[0, 1]^2$. We see that EIC and CMES-IBO outperformed other methods, and in particular, CMES is clearly worse than CMES-IBO. Additionally, we run the experiments with the ‘single constraint’ transformation of multiple constraints described in Section 5, in which a GP fits to $\min_{c=1, \dots, 10} (g_c(\mathbf{x}) - z_c)$ as one constraint. The results shown by dashed lines indicate that this approach deteriorated performance compared with their multiple constraints counterpart.

Small C benchmarks (b)-(c): We used benchmark functions in CBO literature [Gardner et al., 2014, Hernández-Lobato et al., 2015]. The detailed form of each function is in Appendix J. Gardner1 [Gardner et al., 2014] is a simple test problem constructed by sine and cosine functions. The Hartmann6 function is used in [Letham et al., 2019], which has a relatively high input dimension ($d = 6$). In Gardner1, the utility gap of CMES-IBO converged clearly faster than the other methods. In Hartmann6, CMES-IBO and CMES showed more significant decreases of the utility gaps than the other methods, and in particular, CMES-IBO shows a much faster decrease.

Large C benchmarks (d)-(e): We here employed benchmark problems called G7 ($C = 8$ and $d = 8$) and G10 ($C = 6$ and $d = 10$), for which the detailed definitions can be found in [Liang et al., 2006]. In CBO literature, empirical evaluations are typically performed with $C \leq 2$, and thus, the settings $C = 8$ and 6 are relatively large. Moreover, the input dimension d is also large, and the estimated ratio between the feasible region and the input space is very small (less than 0.001%) [Liang et al., 2006]. We can see that CMES-

IBO has superior or comparable to the other methods in all the plots. Note that the slow convergence of PESC can be because Spearmint does not employ the linear kernel though these test functions contain linear functions. In G7, although the utility gap of CMES was not lower than about 10, CMES-IBO converged to a lower value.

Real-world problem (f): We used a reactor network design problem ($d = 6$) [Manousiouthakis and Sourlas, 1992, Kumar et al., 2020], in which the concentration of the product from a sequence of two continuously stirred tank reactors is optimized with capital cost and physical phenomenon constraints. This problem has one inequality constraint and four equality constraints, and we replaced each equality constraint with two inequality constraints, by which we have $C = 9$ inequality constraints. Since the equality constraints cannot be strictly satisfied when evaluating the utility gap, we set the tolerance error as 10^{-3} . We can see that CMES-IBO also shows faster convergence than other methods in this problem.

Parallel Querying: For the parallel setting, we parallelize EIC and TSC (see Appendix J for detail) and set the number of parallel queries $Q = 3$. The prefix ‘P-’ indicates a parallelized variant of each method (e.g., P-EIC and P-CMES). The results are shown in Figure 4. Here, G7 and G10 benchmarks were used, and we see that, similarly to the sequential case, CMES-IBO shows efficient convergences compared with the other methods.

Additional evaluations for different benchmark functions, different sample sizes K , and the correlated extension are shown in Appendix K.

7 Conclusion

We proposed an information-theoretic constrained Bayesian optimization method called CMES-IBO, derived from a lower bound of the MI. We showed its several desired properties, such as the interpretation of the infeasible case, non-negativity, and the bounds of the estimation variability. Moreover, we extended CMES-IBO to the parallel setting. The effectiveness of our proposed method was shown through various benchmark functions and a real-world problem.

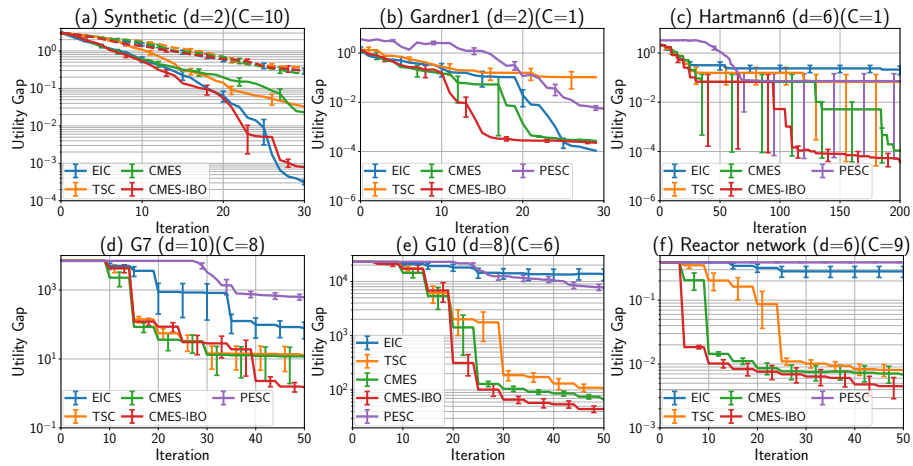


Figure 3: Utility gap in sequential querying (average and standard error). The dashed lines in the synthetic function experiment represent the ‘single constraint’ counterpart of each method that has the same color.

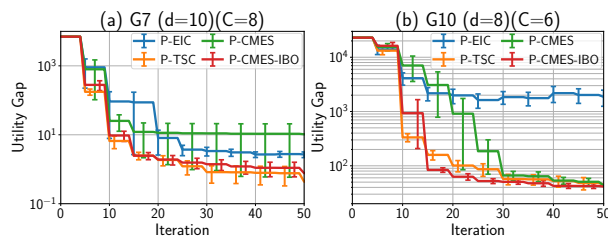


Figure 4: Utility gap in parallel querying (average and standard error).

Acknowledgments

This work was supported by MEXT KAKENHI 17H04694, 18K04700, JSPS KAKENHI Grant Number JP12J34567, and RIKEN Junior Research Associate Program.

References

- Milton Abramowitz and Irene A. Stegun. *Handbook of Mathematical Functions with Formulas, Graphs, and Mathematical Tables*. Dover, ninth Dover printing, tenth GPO printing edition, 1964.
- Setareh Ariaifar, Jaume Coll-Font, Dana Brooks, and Jennifer Dy. ADMMBO: Bayesian optimization with unknown constraints using ADMM. *Journal of Machine Learning Research*, 20(123):1–26, 2019.
- Aleksandr Beknazaryan, Xin Dang, and Hailin Sang. On mutual information estimation for mixed-pair random variables. *Statistics and Probability Letters*, 148:9–16, 2019.
- Syrine Belakaria, Aryan Deshwal, and Janardhan Rao Doppa. Max-value entropy search for multi-objective Bayesian optimization. In *Advances in Neural Information Processing Systems 32*, pages 7825–7835. Curran Associates, Inc., 2019.
- Syrine Belakaria, Aryan Deshwal, and Janardhan Rao Doppa. Max-value entropy search for multi-objective Bayesian optimization with constraints. *arXiv:2009.01721*, 2020.
- Stephen Boyd and Lieven Vandenberghe. *Convex optimization*. Cambridge university press, 2004.
- George Casella and Roger Berger. *Statistical Inference*. Duxbury advanced series in statistics and decision sciences. Thomson Learning, 2002.
- John W. Chinneck. *Feasibility and Infeasibility in Optimization: Algorithms and Computational Methods*. Springer Publishing Company, Incorporated, 2007.
- Thomas M. Cover and Joy A. Thomas. *Elements of Information Theory*. Wiley-Interscience, 2006.
- David Eriksson and Matthias Poloczek. Scalable constrained Bayesian optimization. In *Proceedings of The 24th International Conference on Artificial Intelligence and Statistics*, volume 130, pages 730–738. PMLR, 2021.
- Daniel Fernández-Sánchez, Eduardo C. Garrido-Merchán, and Daniel Hernández-Lobato. Max-value entropy search for multi-objective Bayesian optimization with constraints. *arXiv:2011.01150*, 2020.
- Manjunath B G and Stefan Wilhelm. Moments calculation for the doubly truncated multivariate normal density. *arXiv:1206.5387*, 2012.

- Jacob Gardner, Matt Kusner, Zhixiang, Kilian Weinberger, and John Cunningham. Bayesian optimization with inequality constraints. In *Proceedings of the 31st International Conference on Machine Learning*, volume 32, pages 937–945. PMLR, 2014.
- Michael A. Gelbart, Jasper Snoek, and Ryan P. Adams. Bayesian optimization with unknown constraints. In *Proceedings of the 30th Conference on Uncertainty in Artificial Intelligence*, page 250–259. AUAI Press, 2014.
- Alan Genz. Numerical computation of multivariate normal probabilities. *Journal of Computational and Graphical Statistics*, 1:141–150, 1992.
- GPy. GPy: A Gaussian process framework in python. <http://github.com/SheffieldML/GPy>, since 2012.
- Robert Gramacy and Herbert Lee. Optimization under unknown constraints. *Bayesian Statistics 9*, 2010.
- Robert B. Gramacy, Genetha A. Gray, Sébastien Le Digabel, Herbert K. H. Lee, Pritam Ranjan, Garth Wells, and Stefan M. Wild. Modeling an augmented Lagrangian for blackbox constrained optimization. *Technometrics*, 58(1):1–11, 2016.
- José Miguel Hernández-Lobato, Matthew W. Hoffman, and Zoubin Ghahramani. Predictive entropy search for efficient global optimization of black-box functions. In *Advances in Neural Information Processing Systems 27*, page 918–926. Curran Associates, Inc., 2014.
- José Miguel Hernández-Lobato, Michael A. Gelbart, Matthew W. Hoffman, Ryan P. Adams, and Zoubin Ghahramani. Predictive entropy search for Bayesian optimization with unknown constraints. In *Proceedings of the 32th International Conference on Machine Learning*, volume 37, pages 1699–1707. PMLR, 2015.
- José Miguel Hernández-Lobato, Michael A. Gelbart, Ryan P. Adams, Matthew W. Hoffman, and Zoubin Ghahramani. A general framework for constrained Bayesian optimization using information-based search. *Journal of Machine Learning Research*, 17(160):1–53, 2016.
- William C. Horrace. Some results on the multivariate truncated normal distribution. *Journal of Multivariate Analysis*, 94(1):209–221, 2005.
- Steven G. Johnson. The NLOpt nonlinear-optimization package. <http://github.com/stevengj/nlopt>, since 2008.
- Kirthevasan Kandasamy, Akshay Krishnamurthy, Jeff Schneider, and Barnabas Póczos. Parallelised Bayesian optimisation via Thompson sampling. In *Proceedings of the 21st International Conference on Artificial Intelligence and Statistics*, volume 84, pages 133–142. PMLR, 2018.

- Abhishek Kumar, Guohua Wu, Mostafa Z Ali, Rammohan Mallipeddi, Ponnuthurai Nagarathnam Suganthan, and Swagatam Das. A test-suite of non-convex constrained optimization problems from the real-world and some baseline results. *Swarm and Evolutionary Computation*, 56:100693, 2020.
- Benjamin Letham, Brian Karrer, Guilherme Ottoni, and Eytan Bakshy. Constrained Bayesian optimization with noisy experiments. *Bayesian Anal.*, 14(2):495–519, 2019.
- Jing Liang, Thomas Runarsson, Efrén Mezura-Montes, M. Clerc, Ponnuthurai Suganthan, Carlos Coello, and Kalyan Deb. Problem definitions and evaluation criteria for the CEC 2006 special session on constrained real-parameter optimization. *Nanyang Technological University, Tech. Rep.*, 41, 2006.
- Wei-Liem Loh. On Latin hypercube sampling. *Ann. Statist.*, 24(5):2058–2080, 1996.
- Vasilios Manousiouthakis and Dennis Sourlas. A global optimization approach to rationally constrained rational programming. *Chemical Engineering Communications*, 115(1):127–147, 1992.
- Joseph Victor Michalowicz, Jonathan M. Nichols, and Frank Bucholtz. *Handbook of Differential Entropy*. Chapman and Hall/CRC, 2014.
- Henry B. Moss, David S. Leslie, Javier Gonzalez, and Paul Rayson. GIBBON: General-purpose information-based Bayesian optimisation. *arXiv:2102.03324*, 2021.
- Chandra Nair, Balaji Prabhakar, and Devavrat Shah. On entropy for mixtures of discrete and continuous variables. *arXiv:cs/0607075*, 2007.
- Valerio Perrone, Iaroslav Shcherbatyi, Rodolphe Jenatton, Cedric Archambeau, and Matthias Seeger. Constrained Bayesian optimization with max-value entropy search. *arXiv:1910.07003*, 2019.
- Victor Picheny. A Stepwise uncertainty reduction approach to constrained global optimization. In *Proceedings of the 17th International Conference on Artificial Intelligence and Statistics*, volume 33, pages 787–795. PMLR, 2014.
- Victor Picheny, Robert B Gramacy, Stefan Wild, and Sebastien Le Digabel. Bayesian optimization under mixed constraints with a slack-variable augmented Lagrangian. In *Advances in Neural Information Processing Systems 29*, pages 1435–1443. Curran Associates, Inc., 2016.
- Ali Rahimi and Benjamin Recht. Random features for large-scale kernel machines. In *Advances in Neural Information Processing Systems 20*, pages 1177–1184. Curran Associates, Inc., 2008.
- Carl Edward Rasmussen and Christopher K. I. Williams. *Gaussian Processes for Machine Learning (Adaptive Computation and Machine Learning)*. The MIT Press, 2005.
- Matthias Schonlau, William J. Welch, and Donald R. Jones. *Global versus local search in constrained optimization of computer models*, volume 34 of *Lecture Notes–Monograph Series*, pages 11–25. Institute of Mathematical Statistics, 1998.

- Jasper Snoek. *Bayesian Optimization and Semiparametric Models with Applications to Assistive Technology*. University of Toronto, 2013.
- Shinya Suzuki, Shion Takeno, Tomoyuki Tamura, Kazuki Shitara, and Masayuki Karasuyama. Multi-objective Bayesian optimization using Pareto-frontier entropy. In *Proceedings of the 37th International Conference on Machine Learning*, volume 119, pages 9279–9288. PMLR, 2020.
- Krister Svanberg. A class of globally convergent optimization methods based on conservative convex separable approximations. *SIAM J. on Optimization*, 12(2):555–573, 2002.
- Shion Takeno, Hitoshi Fukuoka, Yuhki Tsukada, Toshiyuki Koyama, Motoki Shiga, Ichiro Takeuchi, and Masayuki Karasuyama. Multi-fidelity Bayesian optimization with max-value entropy search and its parallelization. In *Proceedings of the 37th International Conference on Machine Learning*, volume 119, pages 9334–9345. PMLR, 2020.
- Roman Vershynin. *High-Dimensional Probability: An Introduction with Applications in Data Science*. Cambridge Series in Statistical and Probabilistic Mathematics. Cambridge University Press, 2018.
- Zi Wang and Stefanie Jegelka. Max-value entropy search for efficient Bayesian optimization. In *Proceedings of the 34th International Conference on Machine Learning*, volume 70, pages 3627–3635. PMLR, 2017.
- James Wilson, Frank Hutter, and Marc Deisenroth. Maximizing acquisition functions for Bayesian optimization. In *Advances in Neural Information Processing Systems 31*, page 9906–9917. Curran Associates, Inc., 2018.

A Definition of Gaussian Processes

We use standard GP models [Rasmussen and Williams, 2005] for modeling f and g_1, \dots, g_C . Suppose that the observations are contaminated with additive Gaussian noises as $y_{\mathbf{x}}^{(f)} = f(\mathbf{x}) + \varepsilon$ and $y_{\mathbf{x}}^{(g_c)} = g_c(\mathbf{x}) + \varepsilon$ for $\forall c$, where $\varepsilon \sim \mathcal{N}(0, \sigma_{\text{noise}}^2)$. For the GP prior, we employ $\mathcal{GP}(0, k(\mathbf{x}, \mathbf{x}'))$, which indicates that the prior mean is 0 and covariance is specified by a kernel function $k: \mathcal{X} \times \mathcal{X} \mapsto \mathbb{R}$. Then, the predictive distribution for $f(\mathbf{x})$ given $\mathcal{D}_n^{(f)} = \{(\mathbf{x}_i, y_{\mathbf{x}_i}^{(f)})\}_{i=1}^n$ is derived as follows:

$$\begin{aligned} f(\mathbf{x}) | \mathcal{D}_n^{(f)} &\sim \mathcal{N}(\mu_n^{(f)}(\mathbf{x}), \sigma_n^{(f)2}(\mathbf{x})), \\ \mu_n^{(f)}(\mathbf{x}) &= \mathbf{k}^\top (\mathbf{K} + \sigma_{\text{noise}}^2 \mathbf{I})^{-1} \mathbf{y}^{(f)}, \\ \sigma_n^{(f)2}(\mathbf{x}) &= k(\mathbf{x}, \mathbf{x}) - \mathbf{k}^\top (\mathbf{K} + \sigma_{\text{noise}}^2 \mathbf{I})^{-1} \mathbf{k}, \end{aligned}$$

where $\mathbf{y}^{(f)} = (y_{\mathbf{x}_1}^{(f)}, \dots, y_{\mathbf{x}_n}^{(f)})^\top$, $\mathbf{k} = (k(\mathbf{x}, \mathbf{x}_1), \dots, k(\mathbf{x}, \mathbf{x}_n))^\top$, $\mathbf{K} \in \mathbb{R}^{n \times n}$ is a kernel matrix whose (i, j) element is defined as $k(\mathbf{x}_i, \mathbf{x}_j)$, and $\mathbf{I} \in \mathbb{R}^{n \times n}$ is the identity matrix. The predictive distributions of g_c can be obtained in the same way using the observations $y_{\mathbf{x}_1}^{(g_c)}, \dots, y_{\mathbf{x}_n}^{(g_c)}$. Note that, for simplicity, we here assume the same kernels and noise variances for all the functions, but both the settings can be changed depending on the function.

B Derivation of Information Lower Bound

Since f_* follows the mixture distribution of discrete and continuous random variables, the MI can be defined as follows [Nair et al., 2007, Beknazaryan et al., 2019]:

$$I(\mathbf{h}_{\mathbf{x}}; f_*) = \mathbb{E}_{f_*} \left[\int p(\mathbf{h}_{\mathbf{x}} | f_*) \log \frac{p(\mathbf{h}_{\mathbf{x}} | f_*)}{p(\mathbf{h}_{\mathbf{x}})} d\mathbf{h}_{\mathbf{x}} \right],$$

where the expectation regarding to f_* can be expanded as

$$\begin{aligned} \mathbb{E}_{f_*} \left[\int p(\mathbf{h}_{\mathbf{x}} | f_*) \log \frac{p(\mathbf{h}_{\mathbf{x}} | f_*)}{p(\mathbf{h}_{\mathbf{x}})} d\mathbf{h}_{\mathbf{x}} \right] &= \Pr(f_* = -\infty) \int p(\mathbf{h}_{\mathbf{x}} | f_* = -\infty) \log \frac{p(\mathbf{h}_{\mathbf{x}} | f_* = -\infty)}{p(\mathbf{h}_{\mathbf{x}})} d\mathbf{h}_{\mathbf{x}} \\ &\quad + \Pr(f_* \neq -\infty) \int p(f_* | f_* \neq -\infty) \int p(\mathbf{h}_{\mathbf{x}} | f_*) \log \frac{p(\mathbf{h}_{\mathbf{x}} | f_*)}{p(\mathbf{h}_{\mathbf{x}})} d\mathbf{h}_{\mathbf{x}} df_*. \end{aligned}$$

Then, our information lower bound can be derived as follows:

$$\begin{aligned} I(\mathbf{h}_{\mathbf{x}}; f_*) &= \mathbb{E}_{f_*} \left[\int p(\mathbf{h}_{\mathbf{x}} | f_*) \log \frac{p(\mathbf{h}_{\mathbf{x}} | f_*)}{p(\mathbf{h}_{\mathbf{x}})} d\mathbf{h}_{\mathbf{x}} \right] \\ &= \mathbb{E}_{f_*} \left[\int p(\mathbf{h}_{\mathbf{x}} | f_*) \left(\log \frac{q(\mathbf{h}_{\mathbf{x}})}{p(\mathbf{h}_{\mathbf{x}})} + \log \frac{p(\mathbf{h}_{\mathbf{x}} | f_*)}{q(\mathbf{h}_{\mathbf{x}})} \right) d\mathbf{h}_{\mathbf{x}} \right] \\ &= \mathbb{E}_{f_*} \left[\int p(\mathbf{h}_{\mathbf{x}} | f_*) \log \frac{q(\mathbf{h}_{\mathbf{x}})}{p(\mathbf{h}_{\mathbf{x}})} d\mathbf{h}_{\mathbf{x}} + D_{\text{KL}}(p(\mathbf{h}_{\mathbf{x}} | f_*) || q(\mathbf{h}_{\mathbf{x}})) \right] \\ &\geq \mathbb{E}_{f_*} \left[\int p(\mathbf{h}_{\mathbf{x}} | f_*) \log \frac{q(\mathbf{h}_{\mathbf{x}})}{p(\mathbf{h}_{\mathbf{x}})} d\mathbf{h}_{\mathbf{x}} \right] \\ &= \mathbb{E}_{f_*} \left[\int p(\mathbf{h}_{\mathbf{x}} | f_*) \log \frac{p(\mathbf{h}_{\mathbf{x}} | \mathbf{h}_{\mathbf{x}} \in \bar{\mathcal{A}}_{f_*})}{p(\mathbf{h}_{\mathbf{x}})} d\mathbf{h}_{\mathbf{x}} \right]. \end{aligned} \tag{13}$$

In the last line, we replace $q(\mathbf{h}_x)$ with $p(\mathbf{h}_x|\mathbf{h}_x \in \overline{\mathcal{A}}_{f_*})$ as defined in (4). Here, from the definition of f_* , we see $p(\mathbf{h}_x|f_*) = p(\mathbf{h}_x|\mathbf{h}_x \in \overline{\mathcal{A}}_{f_*}) = 0$ for $\mathbf{h}_x \in \mathcal{A}_{f_*}$. Additionally, in information theory, $0 \log 0$ is treated as zero based on that $\lim_{x \rightarrow 0} x \log x = 0$ [Cover and Thomas, 2006]. Thus, we obtain

$$\begin{aligned}
(13) &= \mathbb{E}_{f_*} \left[\int_{\overline{\mathcal{A}}_{f_*}} p(\mathbf{h}_x|f_*) \log \frac{p(\mathbf{h}_x)}{(1 - Z_{\mathbf{x}}(f_*))p(\mathbf{h}_x)} d\mathbf{h}_x \right] \\
&= -\mathbb{E}_{f_*} \left[\int_{\overline{\mathcal{A}}_{f_*}} p(\mathbf{h}_x|f_*) \log(1 - Z_{\mathbf{x}}(f_*)) d\mathbf{h}_x \right] \\
&= -\mathbb{E}_{f_*} \left[\log(1 - Z_{\mathbf{x}}(f_*)) \int_{\overline{\mathcal{A}}_{f_*}} p(\mathbf{h}_x|f_*) d\mathbf{h}_x \right] \\
&= -\mathbb{E}_{f_*} [\log(1 - Z_{\mathbf{x}}(f_*))].
\end{aligned}$$

C Details of Parallelization

In this section, we provide the detailed derivation for the parallel setting omitted in the main paper. We assume that Q workers are available by which we can select Q queries as a batch at every iteration. Let $\mathcal{X}_q := \{\mathbf{x}^{(1)}, \dots, \mathbf{x}^{(q)}\}$ be a set of input queries and $\mathcal{H}_q := \{\mathbf{h}_{\mathbf{x}^{(1)}}, \dots, \mathbf{h}_{\mathbf{x}^{(q)}}\}$ be a set of output vectors for an integer $1 \leq q \leq Q$. A naïve extension is to maximize MI between \mathcal{H}_Q and f_* , i.e., $\text{MI}(\mathcal{H}_Q; f_*)$, with respect to the queries \mathcal{X}_Q . However, this approach results in a Qd dimensional acquisition function maximization, which is often extremely hard. Instead, we propose a greedy approximation of $\max_{\mathcal{X}_Q} \text{MI}(\mathcal{H}_Q; f_*)$ using the *conditional mutual information* (CMI).

The q -th step of our greedy selection is defined as $\arg \max_{\mathbf{x}^{(q)}} \text{MI}(\mathcal{H}_q; f_*)$, where $\mathbf{x}^{(1)}, \dots, \mathbf{x}^{(q-1)}$ are already fixed by the previous steps. This procedure maximizes the additional information gain produced by $\mathbf{h}_{\mathbf{x}^{(q)}}$, which can be seen through the following expansion:

$$\text{MI}(\mathcal{H}_q; f_*) = \text{MI}(\mathcal{H}_{q-1}; f_*) + \text{CMI}(\mathbf{h}_{\mathbf{x}^{(q)}}; f_* | \mathcal{H}_{q-1}),$$

where the second term is $\text{CMI}(\mathbf{h}_{\mathbf{x}^{(q)}}; f_* | \mathcal{H}_{q-1}) := \mathbb{E}_{\mathcal{H}_{q-1}} [\text{MI}(\mathbf{h}_{\mathbf{x}^{(q)}}; f_* | \mathcal{H}_{q-1})]$. Importantly, the first term does not depend on $\mathbf{x}^{(q)}$ anymore. Therefore, we obtain $\arg \max_{\mathbf{x}^{(q)}} \text{MI}(\mathcal{H}_q; f_*) = \arg \max_{\mathbf{x}^{(q)}} \text{CMI}(\mathbf{h}_{\mathbf{x}^{(q)}}; f_* | \mathcal{H}_{q-1})$, which means that the greedy selection can be performed by the maximization of CMI.

Our lower bound approach used in (6) can be applied to CMI as follows:

$$\text{CMI}(\mathbf{h}_{\mathbf{x}^{(q)}}; f_* | \mathcal{H}_{q-1}) \geq -\mathbb{E}_{\mathcal{H}_{q-1}, f_*} [\log(1 - Z_{\mathbf{x}}(f_* | \mathcal{X}_{q-1}))] =: L_{\text{par}}(\mathbf{x}^{(q)}), \quad (8)$$

where $Z_q := \Pr(\mathbf{h}_{\mathbf{x}^{(q)}} \in \mathcal{A} | \mathcal{X}_{q-1}, \mathcal{H}_{q-1})$. The derivation of this lower bound is omitted because it is almost identical with the sequential case (see Appendix B). Suppose that $m_q^{(f)}(\mathbf{x})$ and $s_q^{(f)}(\mathbf{x})$ are the predictive mean and variance of $f(\mathbf{x})$ after conditioning by \mathcal{H}_{q-1} , respectively, and that $m_q^{(g_c)}(\mathbf{x})$ and $s_q^{(g_c)}(\mathbf{x})$ are those for $g_c(\mathbf{x})$. Then, from the independence assumption, $Z_q = (1 - \Phi(\eta_q^{(f)}(\mathbf{x}^{(q)}))) \prod_{c=1}^C (1 - \Phi(\eta_q^{(g_c)}(\mathbf{x}^{(q)})))$, where $\eta_q^{(f)}(\mathbf{x}^{(q)}) = (f_* - m_q^{(f)}(\mathbf{x}^{(q)}))/s_q^{(f)}(\mathbf{x}^{(q)})$ and $\eta_q^{(g_c)}(\mathbf{x}^{(q)}) = (z_c - m_q^{(g_c)}(\mathbf{x}^{(q)}))/s_q^{(g_c)}(\mathbf{x}^{(q)})$, $c = 1, \dots, C$. By applying the Monte Carlo estimation to the expectation in (8), we obtain the acquisition function for the

q -th query as

$$\alpha_t^{\text{IBO}}(\mathbf{x}^{(q)}|\mathcal{X}_{q-1}) = -\frac{1}{K} \sum_{(f_*, \mathcal{H}_{q-1}) \in \mathcal{J}} \log(1 - Z_{\mathbf{x}}(f_*|\mathcal{X}_{q-1})), \quad (9)$$

where \mathcal{J} is a set of K sampled (f_*, \mathcal{H}_{q-1}) from the current GPs.

D Proof of Theorem 4.1

Let $f_{*(1)}, \dots, f_{*(K)}$ be i.i.d. random variables sampled from the distribution of f_* , and let $D_k := -\log(1 - \Pr(\mathbf{h}_{\mathbf{x}} \in \mathcal{A}_{f_{*(k)}}))$, where $\mathcal{A}_{f_{*(k)}} := (f_{*(k)}, \infty) \times (z_1, \infty) \times \dots \times (z_C, \infty)$ for $\forall k \in \{1, \dots, K\}$. Then, our acquisition function can be written as

$$\alpha_t^{\text{IBO}}(\mathbf{x}) = \frac{1}{K} \sum_{k=1}^K D_k.$$

For any $b \in \mathbb{R} \cup \{-\infty\}$, the following inequality holds:

$$\Pr(\mathbf{h}_{\mathbf{x}} \in \mathcal{B}) \leq \Pr(f_* > b),$$

where $\mathcal{B} := (b, \infty) \times (z_1, \infty) \times \dots \times (z_C, \infty)$. This is because $\mathbf{h}_{\mathbf{x}} \in \mathcal{B}$ implies that (i) $\mathcal{X}_{\text{feasible}}$ is not empty since at least \mathbf{x} is feasible and (ii) $f_* = \max_{\mathbf{x}' \in \mathcal{X}_{\text{feasible}}} f(\mathbf{x}') \geq f(\mathbf{x}) > b$. By substituting the sampled $f_{*(1)}, \dots, f_{*(K)}$ into b , we see

$$\Pr(\mathbf{h}_{\mathbf{x}} \in \mathcal{A}_{f_{*(k)}}) \leq \Pr(f_* > f_{*(k)}),$$

and

$$1 - \Pr(\mathbf{h}_{\mathbf{x}} \in \mathcal{A}_{f_{*(k)}}) \geq 1 - \Pr(f_* > f_{*(k)}) = F_*(f_{*(k)}), \quad (14)$$

where $F_*(b) := \Pr(f_* \leq b)$ is CDF of f_* .

Let us consider the distribution of $F_*(f_{*(k)})$ induced by $f_{*(k)}$. Define $\tau := \Pr(f_* = -\infty)$. Then, $f_{*(k)} = -\infty$ with probability τ because $f_{*(k)}$ is a random sample of f_* . This implies $F_*(f_{*(k)}) = \Pr(f_* = -\infty) = \tau$ with probability τ . Moreover, the CDF of $F_*(f_{*(k)})$, defined as $\Pr(F_*(f_{*(k)}) \leq \alpha)$, is continuous for $\alpha \in (\tau, 1)$. Thus, as with the probability integral transform (e.g., see [Casella and Berger, 2002]), $\Pr(F_*(f_{*(k)}) \leq \alpha)$ can be obtained as

$$\begin{aligned} \Pr(F_*(f_{*(k)}) \leq \alpha) &= \Pr(F_*^{-1}(F_*(f_{*(k)})) \leq F_*^{-1}(\alpha)) \\ &= \Pr(f_{*(k)} \leq F_*^{-1}(\alpha)) \\ &= F_*(F_*^{-1}(\alpha)) \\ &= \alpha, \end{aligned}$$

where $F_*^{-1}(\cdot)$ is the quantile function of f_* . Consequently, CDF of $F_*(f_{*(k)})$ is obtained as,

$$\Pr(F_*(f_{*(k)}) \leq \alpha) = \begin{cases} 0 & \text{if } \alpha < \tau, \\ \alpha & \text{if } \alpha \geq \tau. \end{cases}$$

From above, $F_*(f_{*(k)}) = \tau$ with probability τ , and $F_*(f_{*(k)}) \sim \text{Unif}(\tau, 1)$ with probability $1 - \tau$. Then, we define the random variable U_k as follows:

$$U_k = \begin{cases} \tilde{U}_k & \text{if } f_{*(k)} = -\infty, \\ F_*(f_{*(k)}) & \text{if } f_{*(k)} \neq -\infty, \end{cases}$$

where $\tilde{U}_k \sim \text{Unif}(0, \tau)$. In this definition, we have $U_k \sim \text{Unif}(0, \tau)$ with probability τ , and $U_k \sim \text{Unif}(\tau, 1)$ with probability $1 - \tau$. Therefore, $U_k \sim \text{Unif}(0, 1)$. Since $F_*(f_{*(k)}) \geq U_k$ from the definition, by combining (14), we obtain

$$1 - \Pr(\mathbf{h}_{\mathbf{x}} \in \mathcal{A}_{f_{*(k)}}) \geq F_*(f_{*(k)}) \geq U_k. \quad (15)$$

From this inequality and the monotonicity of logarithm, we can transform

$$D_k = -\log(1 - \Pr(\mathbf{h}_{\mathbf{x}} \in \mathcal{A}_{f_{*(k)}})) \leq -\log(F_*(f_{*(k)})) \leq -\log(U_k) =: M_k.$$

D_k and M_k are nonnegative random variables, and $\Pr(D_k \leq M_k) = 1$. Hence, we see that $0 \leq \mathbb{E}_{\mathcal{F}_*}[D_k] \leq \mathbb{E}_{\mathcal{F}_*}[M_k]$, $\mathbb{E}_{\mathcal{F}_*}[D_k^2] \leq \mathbb{E}_{\mathcal{F}_*}[M_k^2]$, and $\Pr(D_k \geq b) \leq \Pr(M_k \geq b)$ for $\forall b \in \mathbb{R}$.

We will show that variance and concentration bounds for D_k can be derived from that of M_k . Using the inverse probability integral transform [Casella and Berger, 2002], $-\log(U_k)$ follows an exponential distribution with the rate parameter $\lambda = 1$:

$$M_k = -\log(U_k) \sim \exp(\lambda = 1).$$

Therefore, $\mathbb{E}_{f_{*(k)}}[M_k^2] = 2$, and we can derive the inequality below:

$$\begin{aligned} \mathbb{V}_{f_{*(k)}}[D_k] &= \mathbb{E}_{f_{*(k)}}[D_k^2] - \mathbb{E}_{f_{*(k)}}[D_k]^2 \\ &\leq \mathbb{E}_{f_{*(k)}}[D_k^2] \\ &\leq \mathbb{E}_{f_{*(k)}}[M_k^2] \\ &= 2. \end{aligned}$$

Moreover, we see that D_k satisfies the condition being a *sub-exponential random variable* [Proposition 2.7.1 (a) in Vershynin, 2018], that is,

$$\Pr(|D_k| \geq \xi) = \Pr(D_k \geq \xi) \leq \Pr(M_k \geq \xi) = \exp(-\xi) \text{ for all } \xi \geq 0.$$

Consequently, D_k is a sub-exponential random variable, whose variance is bounded from above $\mathbb{V}_{f_{*(k)}}[D_k] \leq 2$.

We can directly apply Chebyshev’s and Bernstein’s inequalities from the bound of variance and the fact that D_k is a sub-exponential random variable. First, applying Chebyshev’s inequality, we can see immediately

$$\Pr(|\alpha_t^{\text{IBO}}(\mathbf{x}) - L(\mathbf{x})| \geq \xi) \leq \frac{2}{K\xi^2}, \quad (16)$$

for any $\xi \geq 0$. Second, applying Bernstein’s inequality [Corollary 2.8.3 in Vershynin, 2018], we can derive

$$\Pr(|\alpha_t^{\text{IBO}}(\mathbf{x}) - L(\mathbf{x})| \geq \xi) \leq 2 \exp\left[-AK \min\left(\frac{\xi^2}{B^2}, \frac{\xi}{B}\right)\right], \quad (17)$$

where A is a constant and B can be provided as a *sub-exponential norm* [Definition 2.7.5 in Vershynin, 2018] of $D_k - \mathbb{E}_{f_{*(k)}}[D_k]$. For all $t \geq 0$ and $\mathbf{x} \in \mathcal{X}$, the sub-exponential norm $\|D_k - \mathbb{E}_{f_{*(k)}}[D_k]\|_{\psi_1}$ can be bounded as

$$\begin{aligned} \|D_k - \mathbb{E}_{f_{*(k)}}[D_k]\|_{\psi_1} &\leq \|D_k\|_{\psi_1} + \|\mathbb{E}_{f_{*(k)}}[D_k]\|_{\psi_1} && \text{(triangle inequality)} \\ &\leq \|M_k\|_{\psi_1} + \|\mathbb{E}_{f_{*(k)}}[M_k]\|_{\psi_1} && (\Pr(D_k \leq M_k) = 1) \\ &= \|M_k\|_{\psi_1} + \|1\|_{\psi_1} && (\mathbb{E}_{f_{*(k)}}[M_k] = 1) \\ &= 2 + 1/\log 2. && (M_k \sim \exp(\lambda = 1)) \end{aligned}$$

Therefore, B can be set as $2 + 1/\log 2$. Consequently, we can derive Theorem 4.1 combining these two inequalities (16) and (17).

All the above derivations hold even after conditioning by \mathcal{H}_q for the parallel setting. Let $D_k^{(q)} := -\log(1 - \Pr(\mathbf{h}_{\mathbf{x}} \in \mathcal{A}_{f_{*(k)}} | \mathcal{H}_{q-1}))$ and $\alpha_t^{\text{IBO}}(\mathbf{x} | \mathcal{X}_{q-1}) = 1/K \sum_{k=1}^K D_k^{(q)}$. Then, using $U_k^{(q)} \sim \text{Unif}(0, 1)$, we can show that $D_k^{(q)} \leq M_k^{(q)} := -\log(U_k^{(q)})$ from the same derivation. Since $M_k^{(q)}$ obviously follows the exponential distribution, we see that $\mathbb{V}_{\mathcal{J}}[D_k^{(q)}] \leq 2$ and $D_k^{(q)}$ is also still a sub-exponential random variable. The subsequent inequalities can be derived in the same way.

E Discussion on Infeasibility

Here, we discuss the case that sample paths generated for sampling f_* do not have any feasible solution. Perrone et al. [2019] defined f_* as $\max f(\mathbf{x})$, s.t. $g_c(\mathbf{x}) \geq z_c$ for $\forall c = 1, \dots, C$, by which the infeasible case is not considered. However, particularly when the dataset \mathcal{D}_{t-1} does not contain any feasible solution (which typically occurs at the beginning of the optimization), it often occurs that a sample path generated for sampling f_* does not have any feasible solution. An illustrative example is shown in Figure 1 (a), in which the feasible region of the green sample path is empty. In fact, GPs can generate an infeasible sample path, i.e., $\Pr(\mathcal{X}_{\text{feasible}} = \emptyset) > 0$ unless we observe a noiseless feasible solution. Then, there is a possibility that f_* is not defined, by which MI even cannot be theoretically defined. Other than using our definition of f_* (1), another possible approach to avoiding this problem is to assume the existence of feasible solutions in the GPs, but this approach has at least the following three disadvantages. First, this approach ignores uncertainty about the existence of a feasible solution. Identifying the existence of a feasible solution for a given problem is a key issue

in constrained problems (called the feasibility problem [Chinneck, 2007]). However, information gain about feasibility cannot be incorporated in this approach. Second, we need to generate sample paths that have feasible solutions for sampling f_* . A naïve approach is the rejection sampling, in which generated constraint functions are rejected if no feasible solution exists, but this may require a huge number of samplings. Third, the predictive distribution of \mathbf{h}_x under this condition $p(\mathbf{h}_x \mid \text{at least one feasible } \mathbf{x} \text{ exists})$ is not a Gaussian distribution anymore, and is analytically intractable. This makes the entire computational procedures of both CMES-IBO and CMES much more complicated. Perrone et al. [2019] did not mention the above issues at all and used the usual predictive distributions of GPs in the entire acquisition function evaluation without any justification. Note that the same problem exists in the PES-based CBO [Hernández-Lobato et al., 2015, 2016]. On the other hand, our definition of f_* (1) resolves the above issues.

We further discuss how CMES-IBO balances the effect of the objective and constraint functions when infeasible sample paths are generated. For simplicity, we first consider the case of $K = 1$. The acquisition function (7) can be written as $-\log(1 - P_{\text{imp}} \times P_{\text{fea}})$, where $P_{\text{imp}} := \Pr(f(\mathbf{x}) \geq f_*)$ and $P_{\text{fea}} := \prod_{c=1}^C \Pr(g_c(\mathbf{x}) \geq z_c)$. In this criterion, P_{imp} and P_{fea} represent benefits for obtaining a larger value of $f(\mathbf{x})$ and for obtaining a feasible solution, respectively. If the sample path does not have a feasible region, $P_{\text{imp}} = \Pr(f(\mathbf{x}) \geq -\infty) = 1$. Thus, only the probability of being feasible P_{fea} is maximized. On the other hand, when $K > 1$, the balance of the effect of the objective and the constraint functions are balanced through the frequency that sampled constraint functions have a feasible region among K samplings. If the frequency is low, the probability of being feasible has a dominant effect, while if the frequency is high, the effect of the objective function becomes strong. Note that sampled constraint functions can have feasible solutions even when the dataset \mathcal{D}_{t-1} does not contain any feasible solution (as illustrated in Figure 1 (a)).

F Constrained Extension of Conventional Max-value Entropy Search

We here extend cMES [Perrone et al., 2019] to the multiple constraints setting and the parallel setting, and further, we show an example that its approximate MI can be negative.

F.1 Acquisition Function of CMES

Following the conventional MES and cMES [Wang and Jegelka, 2017, Perrone et al., 2019], we transform and approximate MI as below:

$$\begin{aligned} (2) &= H(\mathbf{h}_x) - \mathbb{E}_{f_*} [H(\mathbf{h}_x \mid f_*)] \\ &\approx H(\mathbf{h}_x) - \mathbb{E}_{f_*} [H(\mathbf{h}_x \mid \mathbf{h}_x \in \bar{\mathcal{A}}_{f_*})]. \end{aligned} \quad (10)$$

For the approximation, the conditioning on f_* in the second term is replaced with $\mathbf{h}_x \in \bar{\mathcal{A}}_{f_*}$ following the existing approach [Perrone et al., 2019]. Further, the expectation over $p(f_*)$ in the second term of (10) is also analytically intractable. This expectation can be approximated by the MC method that samples f_*

from $p(f_*)$, for which we employ the same RFF-based approach described in Appendix H.1. Thus, we obtain the following acquisition function as an approximation of (10):

$$\alpha_t^{\text{CMES}}(\mathbf{x}) := H(\mathbf{h}_x) - \frac{1}{K} \sum_{f_* \in \mathcal{F}_*} H(\mathbf{h}_x | \mathbf{h}_x \in \bar{\mathcal{A}}_{f_*}). \quad (18)$$

The first term is easy to calculate because it is the entropy of the multivariate normal distribution. Hence, we need to calculate the entropy in the second term $H(\mathbf{h}_x | \mathbf{h}_x \in \bar{\mathcal{A}}_{f_*})$.

Although Perrone et al. [2019] derived a closed-form of the entropy of this TMN distribution specific for $C = 1$, for $C > 1$, directly evaluating it is not trivial as pointed out by [Fernández-Sánchez et al., 2020]. We show that another analytical representation of this entropy actually can be derived for general C by transforming the domain of the integration as follows:

$$\begin{aligned} H(\mathbf{h}_x | \mathbf{h}_x \in \bar{\mathcal{A}}_{f_*}) &= \int_{\bar{\mathcal{A}}_{f_*}} -\frac{p(\mathbf{h}_x)}{\bar{Z}_x(f_*)} \log \frac{p(\mathbf{h}_x)}{\bar{Z}_x(f_*)} d\mathbf{h}_x \\ &= \int -\frac{p(\mathbf{h}_x)}{\bar{Z}_x(f_*)} \log \frac{p(\mathbf{h}_x)}{\bar{Z}_x(f_*)} d\mathbf{h}_x + \int_{\mathcal{A}_{f_*}} \frac{p(\mathbf{h}_x)}{\bar{Z}_x(f_*)} \log \frac{p(\mathbf{h}_x)}{\bar{Z}_x(f_*)} d\mathbf{h}_x \\ &= \frac{1}{\bar{Z}_x(f_*)} \int -p(\mathbf{h}_x) \log p(\mathbf{h}_x) d\mathbf{h}_x + \frac{1}{\bar{Z}_x(f_*)} \int_{\mathcal{A}_{f_*}} p(\mathbf{h}_x) \log p(\mathbf{h}_x) d\mathbf{h}_x + \log(\bar{Z}_x(f_*)) \\ &= \frac{1}{\bar{Z}_x(f_*)} \int -p(\mathbf{h}_x) \log p(\mathbf{h}_x) d\mathbf{h}_x + \frac{Z_x(f_*)}{\bar{Z}_x(f_*)} \int_{\mathcal{A}_{f_*}} \frac{p(\mathbf{h}_x)}{Z_x(f_*)} \log \frac{p(\mathbf{h}_x)}{Z_x(f_*)} d\mathbf{h}_x + \log(\bar{Z}_x(f_*)) + \frac{Z_x(f_*) \log(Z_x(f_*))}{\bar{Z}_x(f_*)} \\ &= \frac{H(\mathbf{h}_x)}{\bar{Z}_x(f_*)} - \frac{Z_x(f_*)}{\bar{Z}_x(f_*)} \int_{\mathcal{A}_{f_*}} -p(\mathbf{h}_x | \mathbf{h}_x \in \mathcal{A}_{f_*}) \log p(\mathbf{h}_x | \mathbf{h}_x \in \mathcal{A}_{f_*}) d\mathbf{h}_x + \log(\bar{Z}_x(f_*)) + \frac{Z_x(f_*) \log(Z_x(f_*))}{\bar{Z}_x(f_*)} \\ &= \frac{H(\mathbf{h}_x)}{\bar{Z}_x(f_*)} - \frac{Z_x(f_*) H(\mathbf{h}_x | \mathbf{h}_x \in \mathcal{A}_{f_*})}{\bar{Z}_x(f_*)} + \log(\bar{Z}_x(f_*)) + \frac{Z_x(f_*) \log Z_x(f_*)}{\bar{Z}_x(f_*)}, \end{aligned} \quad (19)$$

where TMN $p(\mathbf{h}_x | \mathbf{h}_x \in \mathcal{A}_{f_*})$ is defined as

$$p(\mathbf{h}_x | \mathbf{h}_x \in \mathcal{A}_{f_*}) = \begin{cases} p(\mathbf{h}_x)/Z_x(f_*) & \text{if } \mathbf{h}_x \in \mathcal{A}_{f_*} \\ 0 & \text{otherwise} \end{cases}.$$

In the last equation, $Z_x(f_*)$, $\bar{Z}_x(f_*)$ and $H(\mathbf{h}_x)$ are easy to compute. Although $H(\mathbf{h}_x | \mathbf{h}_x \in \mathcal{A}_{f_*})$ in the second term is still the entropy of TMN, we show the calculation of this entropy in Appendix G for both independent and correlated cases.

Consequently, in the independent case, by substituting (19) into (18) and replacing $H(\mathbf{h}_x)$ and $H(\mathbf{h}_x | \mathbf{h}_x \in \mathcal{A}_{f_*})$ with their closed-forms (shown in Appendix G), we obtain

$$\alpha_t^{\text{CMES}}(\mathbf{x}) = \frac{1}{K} \sum_{f_* \in \mathcal{F}_*} \frac{Z_x(f_*)}{2(1 - Z_x(f_*))} R_{f_*} - \log(1 - Z_x(f_*)),$$

where

$$R_{f_*} := \frac{\gamma_t^{(f)}(\mathbf{x}) \phi(\gamma_t^{(f)}(\mathbf{x}))}{1 - \Phi(\gamma_t^{(f)}(\mathbf{x}))} + \sum_{c=1}^C \frac{\gamma_t^{(g_c)}(\mathbf{x}) \phi(\gamma_t^{(g_c)}(\mathbf{x}))}{1 - \Phi(\gamma_t^{(g_c)}(\mathbf{x}))}.$$

In the correlated case, $H(\mathbf{h}_x)$ and $H(\mathbf{h}_x | \mathbf{h}_x \in \mathcal{A}_{f_*})$ are also replaced with their closed-forms (shown in Appendix G), and we obtain

$$\alpha_t^{\text{CMES}}(\mathbf{x}) = \frac{1}{K} \sum_{f_* \in \mathcal{F}_*} \frac{Z_{\mathbf{x}}(f_*)}{2(1 - Z_{\mathbf{x}}(f_*))} \left(\text{Tr} \left(\boldsymbol{\Sigma}_{t-1}^{-1}(\mathbf{x}) (\boldsymbol{\Sigma}_{t-1}^{\text{TN}}(\mathbf{x}) + \mathbf{d}\mathbf{d}^\top) \right) - C - 1 \right) - \log(1 - Z_{\mathbf{x}}(f_*)), \quad (20)$$

where $\text{Tr}(\cdot)$ is the trace of a matrix, and $\boldsymbol{\mu}_{t-1}(\mathbf{x})$ and $\boldsymbol{\Sigma}_{t-1}(\mathbf{x})$ are the expectation and covariance matrix of \mathbf{h}_x , respectively, and $\boldsymbol{\mu}_{t-1}^{\text{TN}}(\mathbf{x})$ and $\boldsymbol{\Sigma}_{t-1}^{\text{TN}}(\mathbf{x})$ are those for $\mathbf{h}_x | \mathbf{h}_x \in \mathcal{A}_{f_*}$. See Appendix G for details.

F.2 Parallelization of CMES

We can consider the CMI maximization in the same way as CMES-IBO. Suppose that we already select the $q-1$ queries, and we need to select the next q -th query. The CMI can be approximated as

$$\begin{aligned} \mathbb{E}_{\mathcal{H}_{q-1}} [I(\mathbf{h}_{\mathbf{x}^{(q)}}; f_* | \mathcal{H}_{q-1})] &= \mathbb{E}_{\mathcal{H}_{q-1}} [H(\mathbf{h}_{\mathbf{x}^{(q)}} | \mathcal{H}_{q-1})] - \mathbb{E}_{\mathcal{H}_{q-1}, f_*} [H(\mathbf{h}_{\mathbf{x}^{(q)}} | f_*, \mathcal{H}_{q-1})] \\ &\approx \mathbb{E}_{\mathcal{H}_{q-1}} [H(\mathbf{h}_{\mathbf{x}^{(q)}} | \mathcal{H}_{q-1})] - \mathbb{E}_{\mathcal{H}_{q-1}, f_*} [H(\mathbf{h}_{\mathbf{x}^{(q)}} | \mathbf{h}_{\mathbf{x}^{(q)}} \in \bar{\mathcal{A}}_{f_*}, \mathcal{H}_{q-1})] \end{aligned}$$

As described in the main paper, we define $f(\mathbf{x}) | \mathcal{D}_{t-1}, \mathcal{X}_{q-1}, \mathcal{H}_{q-1} \sim \mathcal{N}(m_q^{(f)}(\mathbf{x}), s_q^{(f)2}(\mathbf{x}))$ and $g_c(\mathbf{x}) | \mathcal{D}_{t-1}, \mathcal{X}_{q-1}, \mathcal{H}_{q-1} \sim \mathcal{N}(m_q^{(g_c)}(\mathbf{x}), s_q^{(g_c)2}(\mathbf{x}))$ $c = 1, \dots, C$. Importantly, $s_q^{(f)2}(\mathbf{x}), s_q^{(g_c)2}(\mathbf{x}), \dots, s_q^{(g_C)2}(\mathbf{x})$ only depend on \mathcal{X}_{q-1} , not \mathcal{H}_{q-1} . Thus, given \mathcal{X}_{q-1} , the first term $\mathbb{E}_{\mathcal{H}_{q-1}} [H(\mathbf{h}_{\mathbf{x}^{(q)}} | \mathcal{H}_{q-1})]$ can be calculated analytically. The second term is also calculated in the same manner as CMES with given f_* and \mathcal{H}_{q-1} :

$$H(\mathbf{h}_{\mathbf{x}^{(q)}} | \mathbf{h}_{\mathbf{x}^{(q)}} \in \bar{\mathcal{A}}_{f_*}, \mathcal{H}_{q-1}) = H(\mathbf{h}_{\mathbf{x}^{(q)}} | \mathcal{H}_{q-1}) - \frac{Z_{\mathbf{x}}(f_* | \mathcal{X}_{q-1})}{2(1 - Z_{\mathbf{x}}(f_* | \mathcal{X}_{q-1}))} R_{f_*}^{(q)} + \log(1 - Z_{\mathbf{x}}(f_* | \mathcal{X}_{q-1})),$$

where

$$R_{f_*}^{(q)} := \frac{\eta_q^{(f)}(\mathbf{x}^{(q)}) \phi(\eta_q^{(f)}(\mathbf{x}^{(q)}))}{1 - \Phi(\eta_q^{(f)}(\mathbf{x}^{(q)}))} + \sum_{c=1}^C \frac{\eta_q^{(g_c)}(\mathbf{x}^{(q)}) \phi(\eta_q^{(g_c)}(\mathbf{x}^{(q)}))}{1 - \Phi(\eta_q^{(g_c)}(\mathbf{x}^{(q)}))}.$$

Finally, by applying the MC approximation, we obtain the acquisition function below

$$\alpha_t^{\text{CMES}}(\mathbf{x}^{(q)} | \mathcal{X}_{q-1}) = \frac{1}{|\mathcal{J}|} \sum_{(f_*, \mathcal{H}_{q-1}) \in \mathcal{J}} \frac{Z_{\mathbf{x}}(f_* | \mathcal{X}_{q-1})}{2(1 - Z_{\mathbf{x}}(f_* | \mathcal{X}_{q-1}))} R_{f_*}^{(q)} - \log(1 - Z_{\mathbf{x}}(f_* | \mathcal{X}_{q-1})). \quad (21)$$

We can also derive the acquisition function in the correlated setting, but we omit the detailed derivation.

F.3 Proof of Lemma 4.1

We first prove the following auxiliary lemma:

Lemma F.1. *Let $a(\gamma) := \frac{\gamma \phi(\gamma)}{1 - \Phi(\gamma)}$ for $\gamma \in \mathbb{R}$. Then, $\min_{\gamma \in \mathbb{R}} a(\gamma) < -0.29$.*

Proof. Using the approximation of CDF [26.2.17 in Abramowitz and Stegun, 1964], we obtain

$$\Phi(\gamma) = 1 - \phi(\gamma)(b_1 r + b_2 r^2 + b_3 r^3 + b_4 r^4 + b_5 r^5) + \epsilon(\gamma), \quad (22)$$

where

$$|\epsilon(\gamma)| < 7.5 \times 10^{-8}, r = 1/(1 + p\gamma), p = 0.2316419,$$

$$b_1 = 0.319381530, b_2 = -1.821255978, b_3 = -0.356563782, b_4 = 1.330274429, b_5 = 1.781477937.$$

By substituting (22) into $a(\gamma)$, we obtain

$$a(\gamma) = \frac{\gamma}{b_1 r + b_2 r^2 + b_3 r^3 + b_4 r^4 + b_5 r^5 + \epsilon(\gamma)/\phi(\gamma)} \text{ for } \forall \gamma \in \mathbb{R}.$$

Since $\epsilon(\gamma)/\phi(\gamma) = \sqrt{2\pi}e^{\gamma^2}\epsilon(\gamma) < 9\epsilon(\gamma) < 9 \times 7.5 \times 10^{-8} < 10^{-6}$ for $\gamma \in [-1, 0]$, we obtain an upper bound

$$a(\gamma) < \frac{\gamma}{b_1 r + b_2 r^2 + b_3 r^3 + b_4 r^4 + b_5 r^5 + 10^{-6}} \text{ for } \forall \gamma \in [-1, 0]. \quad (23)$$

This upper bound consist of elementary arithmetic that can be computed without approximations such as the numerical integration. We evaluated this upper bound (23) with 28 digits of precision by *decimal* package (<https://docs.python.org/3/library/decimal.html>) in Python, and we confirmed $\min_{\gamma \in \mathbb{R}} a(\gamma) < a(-0.84) < -0.29$. \square

Next, we prove Lemma 4.1. By using $\log(1 - Z) \geq (1 - \frac{1}{1-Z}) = \frac{-Z}{1-Z}$ for $Z \in [0, 1)$, an upper bound of the CMES acquisition function (11) can be derived as

$$\begin{aligned} & \frac{1}{K} \sum_{f_* \in \mathcal{F}_*} \left\{ \frac{Z_{\mathbf{x}}(f_*)}{2(1 - Z_{\mathbf{x}}(f_*))} \left(\frac{\gamma_t^{(f)}(\mathbf{x})\phi(\gamma_t^{(f)}(\mathbf{x}))}{1 - \Phi(\gamma_t^{(f)}(\mathbf{x}))} + \sum_{c=1}^C \frac{\gamma_t^{(g_c)}(\mathbf{x})\phi(\gamma_t^{(g_c)}(\mathbf{x}))}{1 - \Phi(\gamma_t^{(g_c)}(\mathbf{x}))} \right) - \log(1 - Z_{\mathbf{x}}(f_*)) \right\} \\ & \leq \frac{1}{K} \sum_{f_* \in \mathcal{F}_*} \left\{ \frac{Z_{\mathbf{x}}(f_*)}{2(1 - Z_{\mathbf{x}}(f_*))} \left(\frac{\gamma_t^{(f)}(\mathbf{x})\phi(\gamma_t^{(f)}(\mathbf{x}))}{1 - \Phi(\gamma_t^{(f)}(\mathbf{x}))} + \sum_{c=1}^C \frac{\gamma_t^{(g_c)}(\mathbf{x})\phi(\gamma_t^{(g_c)}(\mathbf{x}))}{1 - \Phi(\gamma_t^{(g_c)}(\mathbf{x}))} \right) - \left(\frac{-Z_{\mathbf{x}}(f_*)}{1 - Z_{\mathbf{x}}(f_*)} \right) \right\} \\ & = \frac{1}{K} \sum_{f_* \in \mathcal{F}_*} \frac{Z_{\mathbf{x}}(f_*)}{(1 - Z_{\mathbf{x}}(f_*))} \left\{ \frac{1}{2} \left(\frac{\gamma_t^{(f)}(\mathbf{x})\phi(\gamma_t^{(f)}(\mathbf{x}))}{1 - \Phi(\gamma_t^{(f)}(\mathbf{x}))} + \sum_{c=1}^C \frac{\gamma_t^{(g_c)}(\mathbf{x})\phi(\gamma_t^{(g_c)}(\mathbf{x}))}{1 - \Phi(\gamma_t^{(g_c)}(\mathbf{x}))} \right) + 1 \right\}. \end{aligned}$$

Since $\frac{Z_{\mathbf{x}}(f_*)}{1 - Z_{\mathbf{x}}(f_*)} \geq 0$, we see that the sign of the above upper bound is determined by

$$s(z_1, \dots, z_C) := \frac{1}{2}a(\gamma_t^{(f)}(\mathbf{x})) + \frac{1}{2} \sum_{c=1}^C a(\gamma_t^{(g_c)}(\mathbf{x})) + 1. \quad (24)$$

Note that s is defined as a function of z_c .

From Lemma F.1, we see

$$\min_{z_1, \dots, z_C} s(z_1, \dots, z_C) < \frac{1}{2}a(\gamma_t^{(f)}(\mathbf{x})) - \frac{0.29C}{2} + 1.$$

Moreover, since f_* is the continuous random variable whose support is \mathbb{R} , the probability that $a(\gamma_t^{(f)}(\mathbf{x}))$ is smaller than -0.29 is also positive: $\Pr(a(\gamma_t^{(f)}(\mathbf{x})) < -0.29) > 0$. Hence, if $0.29(C + 1)/2 > 1$, the probability that (24) becomes minus is not zero. Thus, (24) can be minus when $C > 5$, since $0.29(C + 1)/2 = 0.29(6 + 1)/2 = 2.03/2 > 1$ when $C = 6$.

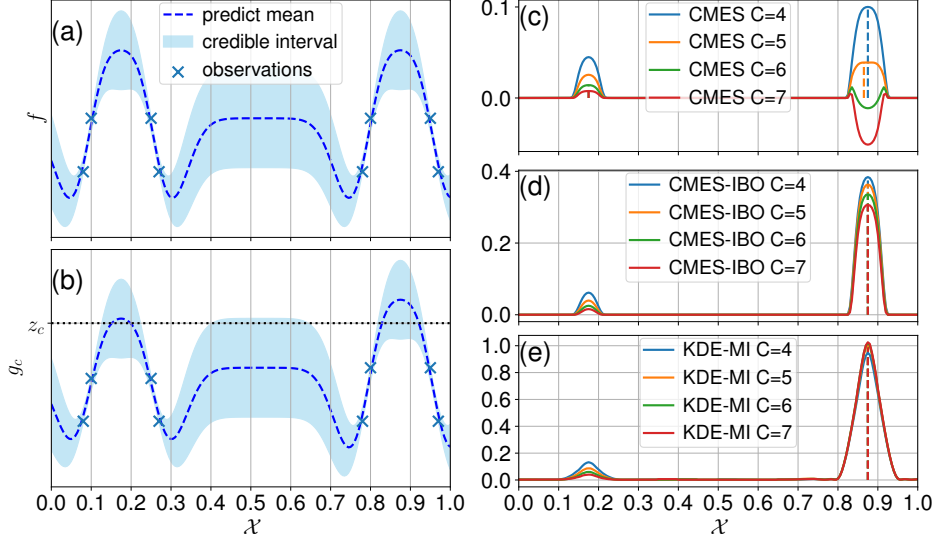


Figure 5: In (a) and (b), the predictions of f and g_c are shown, respectively. The solid line and shaded area represent the predictive mean and the credible interval, and the cross mark is the training data. The horizontal dotted line expresses z_c . In (c)-(e), CMES, CMES-IBO, and the KDE-based MI approximation for $C = 4, 5, 6$, and 7 are shown, and each vertical dotted line indicates the maximum.

F.4 Illustrative Example that CMES Takes a Negative Value

First, we describe the detailed setting of Figure 2 omitted in the main text. In the plots, we have 200 equally spaced grid points as \mathcal{X} . We sampled f_* through the sampling from the predictive multivariate normal distribution on these grid points. The detailed procedure of KDE-MI is as follows. We used the following representation of the MI [Nair et al., 2007] because, in this form, KDE is required only for one dimensional densities:

$$\text{MI}(\mathbf{h}_x; f_*) = \mathbb{E}_{\mathbf{h}_x} \left[\Pr(f_* = -\infty | \mathbf{h}_x) \log \frac{\Pr(f_* = -\infty | \mathbf{h}_x)}{\Pr(f_* = -\infty)} + \Pr(f_* \neq -\infty | \mathbf{h}_x) \log \frac{\Pr(f_* \neq -\infty | \mathbf{h}_x)}{\Pr(f_* \neq -\infty)} \right. \\ \left. + \Pr(f_* \neq -\infty | \mathbf{h}_x) \int p(f_* | \mathbf{h}_x, f_* \neq -\infty) \log \frac{p(f_* | \mathbf{h}_x, f_* \neq -\infty)}{p(f_* | f_* \neq -\infty)} df_* \right],$$

where the expectation over \mathbf{h}_x is approximated by the MC estimation with 10000 samples. The probabilities $\Pr(f_* = -\infty | \mathbf{h}_x)$ and $\Pr(f_* = -\infty)$ are estimated by the percentage of infeasible samples in 10000 samples ($\Pr(f_* \neq -\infty | \mathbf{h}_x)$ and $\Pr(f_* \neq -\infty)$ are estimated in the same way). The one-dimensional density functions $p(f_* | f_* \neq -\infty)$ and $p(f_* | \mathbf{h}_x, f_* \neq -\infty)$ are estimated by KDE fitted to feasible samples among 10000 samples of f_* and $f_* | \mathbf{h}_x$, respectively. Note that $p(f_* | \mathbf{h}_x)$ is approximated by generating 10000 f_* for each MC sample of \mathbf{h}_x . We approximate the one-dimensional integral with respect to f_* in the outer expectation by Gauss-Legendre quadrature. We empirically confirmed that the estimation variance of this procedure was low enough.

Here, we show an additional example in Figure 5, in which the number of the MC samplings in CMES and CMES-IBO is set as $K = 10000$. The other settings are the same as Figure 2. Since we set K as 10000

in Figure 5, we expect that the MC estimation are highly accurate. For CMES, we see that the behavior is slightly improved compared with the case of $K = 10$ in Figure 2 (In particular, the acquisition function of $C = 5$ in Figure 5 (c) is more reasonable than that of Figure 2 (c)). However, in the case of $C = 6$ and 7, CMES still takes negative values. In this example, querying to the inputs around 0.2 and 0.9 are obviously beneficial because both predictions of $f(\mathbf{x})$ and $g_c(\mathbf{x})$ are large. In particular, the inputs around 0.9 can be a better selection than around 0.2 because the probability of being feasible is the highest, while the uncertainty is almost the same as around 0.2. The arg max of KDE-MI and CMES-IBO are the same point around 0.9 regardless of the number of constraints C . On the other hand, the acquisition function values of CMES for a point around 0.9 rapidly decrease with the number of constraints C . Although CMES selects a point around 0.9 for $C = 4$ and 5, but for $C = 6$ and 7, CMES selects a point around 0.2.

G Derivation of Entropy of TMN

In this section, we derive the entropy of TMN truncated by a hyperrectangle $H(\mathbf{h}_x | \mathbf{h}_x \in \mathcal{A}_{f_*})$ for both independent and correlated cases.

G.1 Independent Case

In this case, $H(\mathbf{h}_x | \mathbf{h}_x \in \mathcal{A}_{f_*})$ can be decomposed to the sum of the entropy of each element [Horrace, 2005]:

$$H(\mathbf{h}_x | \mathbf{h}_x \in \mathcal{A}_{f_*}) = H(f(\mathbf{x}) | f(\mathbf{x}) \geq f_*) + \sum_{c=1}^C H(g_c(\mathbf{x}) | g_c(\mathbf{x}) \geq z_c).$$

The analytical form of the entropy of the one-dimensional truncated normal distribution is known [Michalowicz et al., 2014], by which we obtain

$$\begin{aligned} H(f(\mathbf{x}) | f(\mathbf{x}) \geq f_*) &= \log(\sqrt{2\pi e}\sigma_{t-1}^{(f)}(\mathbf{x})(1 - \Phi(\gamma_t^{(f)}(\mathbf{x}))) + \frac{\gamma_t^{(f)}(\mathbf{x})\phi(\gamma_t^{(f)}(\mathbf{x}))}{2(1 - \Phi(\gamma_t^{(f)}(\mathbf{x})))}, \\ H(g_c(\mathbf{x}) | g_c(\mathbf{x}) \geq z_c) &= \log(\sqrt{2\pi e}\sigma_{t-1}^{(g_c)}(\mathbf{x})(1 - \Phi(\gamma_t^{(g_c)}(\mathbf{x}))) + \frac{\gamma_t^{(g_c)}(\mathbf{x})\phi(\gamma_t^{(g_c)}(\mathbf{x}))}{2(1 - \Phi(\gamma_t^{(g_c)}(\mathbf{x})))}. \end{aligned}$$

Moreover, from the independence of each elements of \mathbf{h}_x , we see $H(\mathbf{h}_x) = \log(\sqrt{2\pi e}\sigma_{t-1}^{(f)}(\mathbf{x})) + \sum_{c=1}^C \log(\sqrt{2\pi e}\sigma_{t-1}^{(g_c)}(\mathbf{x}))$. Then, the entropy of TMN is obtained as

$$H(\mathbf{h}_x | \mathbf{h}_x \in \mathcal{A}_{f_*}) = H(\mathbf{h}_x) + \log(Z) + \frac{R}{2},$$

where

$$R = \frac{\gamma_t^{(f)}(\mathbf{x})\phi(\gamma_t^{(f)}(\mathbf{x}))}{1 - \Phi(\gamma_t^{(f)}(\mathbf{x}))} + \sum_{c=1}^C \frac{\gamma_t^{(g_c)}(\mathbf{x})\phi(\gamma_t^{(g_c)}(\mathbf{x}))}{1 - \Phi(\gamma_t^{(g_c)}(\mathbf{x}))}.$$

G.2 Correlated Case

Supposed that \mathbf{h}_x has a correlated distribution defined as

$$\mathbf{h}_x | \mathcal{D}_{t-1} \sim \mathcal{N}(\boldsymbol{\mu}_{t-1}(\mathbf{x}), \boldsymbol{\Sigma}_{t-1}(\mathbf{x})),$$

where $\boldsymbol{\mu}_{t-1}(\mathbf{x})$ and $\boldsymbol{\Sigma}_{t-1}(\mathbf{x})$ can be obtained by an arbitrary multi-output GP model [Rasmussen and Williams, 2005]. Let $\boldsymbol{\mu}_{t-1}^{\text{TN}}(\mathbf{x})$ and $\boldsymbol{\Sigma}_{t-1}^{\text{TN}}(\mathbf{x})$ be the expectation and covariance matrix of $\mathbf{h}_x | \mathbf{h}_x \in \mathcal{A}_{f_*}$, respectively, whose analytical expressions are known [G and Wilhelm, 2012]. We denote $\mathbb{E}_{\mathbf{h}_x | \mathbf{h}_x \in \mathcal{A}_{f_*}}$, which is the expectation with respect to $\mathbf{h}_x | \mathbf{h}_x \in \mathcal{A}_{f_*}$, as \mathbb{E}_{TN} for brevity. Then, we can transform the entropy $H(\mathbf{h}_x | \mathbf{h}_x \in \mathcal{A}_{f_*})$ into

$$\begin{aligned} H(\mathbf{h}_x | \mathbf{h}_x \in \mathcal{A}_{f_*}) &= \mathbb{E}_{\text{TN}} \left[-\log p(\mathbf{h}_x | \mathbf{h}_x \in \mathcal{A}_{f_*}) \right] \\ &= \mathbb{E}_{\text{TN}} \left[-\log \frac{p(\mathbf{h}_x)}{Z} \right] \\ &= \mathbb{E}_{\text{TN}} [-\log p(\mathbf{h}_x)] + \log Z \\ &= \frac{1}{2} \mathbb{E}_{\text{TN}} [(\mathbf{h}_x - \boldsymbol{\mu}_{t-1}(\mathbf{x}))^\top \boldsymbol{\Sigma}_{t-1}^{-1}(\mathbf{x})(\mathbf{h}_x - \boldsymbol{\mu}_{t-1}(\mathbf{x}))] + \frac{1}{2} |2\pi \boldsymbol{\Sigma}_{t-1}(\mathbf{x})| + \log Z \\ &= \frac{1}{2} \text{Tr} \left(\boldsymbol{\Sigma}_{t-1}^{-1}(\mathbf{x}) \underbrace{\mathbb{E}_{\text{TN}} [(\mathbf{h}_x - \boldsymbol{\mu}_{t-1}(\mathbf{x}))(\mathbf{h}_x - \boldsymbol{\mu}_{t-1}(\mathbf{x}))^\top]}_{=: \mathbf{V}} \right) + \frac{1}{2} |2\pi \boldsymbol{\Sigma}_{t-1}(\mathbf{x})| + \log Z, \end{aligned}$$

where $|\cdot|$ is the determinant of a matrix. Further, by using $\mathbf{d} = \boldsymbol{\mu}_{t-1}^{\text{TN}}(\mathbf{x}) - \boldsymbol{\mu}_{t-1}(\mathbf{x})$, we obtain

$$\begin{aligned} \mathbf{V} &= \mathbb{E}_{\text{TN}} [(\mathbf{h}_x - \boldsymbol{\mu}_{t-1}^{\text{TN}}(\mathbf{x}) + \mathbf{d})(\mathbf{h}_x - \boldsymbol{\mu}_{t-1}^{\text{TN}}(\mathbf{x}) + \mathbf{d})^\top] \\ &= \mathbb{E}_{\text{TN}} [(\mathbf{h}_x - \boldsymbol{\mu}_{t-1}^{\text{TN}}(\mathbf{x}))(\mathbf{h}_x - \boldsymbol{\mu}_{t-1}^{\text{TN}}(\mathbf{x}))^\top + \mathbf{d}(\mathbf{h}_x - \boldsymbol{\mu}_{t-1}^{\text{TN}}(\mathbf{x}))^\top + (\mathbf{h}_x - \boldsymbol{\mu}_{t-1}^{\text{TN}}(\mathbf{x}))\mathbf{d}^\top + \mathbf{d}\mathbf{d}^\top] \\ &= \mathbb{E}_{\text{TN}} [(\mathbf{h}_x - \boldsymbol{\mu}_{t-1}^{\text{TN}}(\mathbf{x}))(\mathbf{h}_x - \boldsymbol{\mu}_{t-1}^{\text{TN}}(\mathbf{x}))^\top] + \mathbf{d}\mathbf{d}^\top \\ &= \boldsymbol{\Sigma}_{t-1}^{\text{TN}}(\mathbf{x}) + \mathbf{d}\mathbf{d}^\top, \end{aligned}$$

where we use $\mathbb{E}_{\text{TN}} [(\mathbf{h}_x - \boldsymbol{\mu}_{t-1}^{\text{TN}}(\mathbf{x}))] = 0$. Consequently, we can derive

$$H(\mathbf{h}_x | \mathbf{h}_x \in \mathcal{A}_{f_*}) = \frac{1}{2} \text{Tr} \left(\boldsymbol{\Sigma}_{t-1}^{-1}(\mathbf{x}) (\boldsymbol{\Sigma}_{t-1}^{\text{TN}}(\mathbf{x}) + \mathbf{d}\mathbf{d}^\top) \right) + \frac{1}{2} |2\pi \boldsymbol{\Sigma}_{t-1}(\mathbf{x})| + \log Z.$$

H Computation of CMES and CMES-IBO

In this section, we describe several computational details. First, we present the general algorithm for sequential- and parallel- CMES-IBO in Algo. 1, where sequential CMES-IBO corresponds to the case that $Q = 1$. By replacing (7) and (9) in Algo. 1 with those of CMES (11) and (21), this algorithm can also be seen as the algorithm for sequential- and parallel- CMES.

H.1 Sampling from Posterior

Our proposed method needs to sample the maximum value f_* defined by (1). We employ an approach using random Fourier features (RFF) [Rahimi and Recht, 2008], which has been used in various entropy-based

Algorithm 1 Sequential- and parallel- CMES-IBO.

```

1: function CMES-IBO( $\mathcal{D}_0, \mathcal{X}, Q, K$ )
2:   for  $t = 0, \dots, T$  do
3:     for  $k = 1, \dots, K$  do
4:       Sample  $\tilde{f}_{(k)}, \tilde{g}_{1(k)}, \dots, \tilde{g}_{C(k)}$  from current GPs
5:        $f_{*(k)} \leftarrow \begin{cases} \max_{\mathbf{x} \in \tilde{\mathcal{X}}_{\text{feasible}}} \tilde{f}_{(k)}(\mathbf{x}), & \text{if } \tilde{\mathcal{X}}_{\text{feasible}} \neq \emptyset, \\ -\infty, & \text{otherwise,} \end{cases}$ 
        where  $\tilde{\mathcal{X}}_{\text{feasible}} := \{\mathbf{x} \mid \tilde{g}_c(\mathbf{x}) \geq z_c, c = 1, \dots, C\}$ 
6:     end for
7:      $\mathcal{F}_* = \{f_{*(k)}\}_{k=1}^K$ 
8:      $\mathbf{x}_t^{(1)} \leftarrow \arg \max_{\mathbf{x} \in \mathcal{X}} \alpha_t^{\text{IBO}}(\mathbf{x})$  (7)
9:     if  $Q > 1$  then
10:      for  $q = 2, \dots, Q$  do
11:         $\mathcal{J} = \left\{ \left( f_{*(k)}, \left\{ \left( \tilde{f}_{(k)}(\mathbf{x}_t^{(q')}), \tilde{g}_{1(k)}(\mathbf{x}_t^{(q')}), \dots, \tilde{g}_{C(k)}(\mathbf{x}_t^{(q')}) \right)^\top \right\}_{q'=1}^{q-1} \right) \right\}_{k=1}^K$ 
12:         $\mathbf{x}_t^{(q)} \leftarrow \arg \max_{\mathbf{x} \in \mathcal{X}} \alpha_t^{\text{IBO}}(\mathbf{x} | \mathcal{X}_{q-1})$  (9)
13:      end for
14:    end if
15:    Evaluate  $f, g_1, \dots, g_C$  at  $\mathcal{X}_q$ 
16:    Update  $\mathcal{D}_t^{(f)}, \mathcal{D}_t^{(g_1)}, \dots, \mathcal{D}_t^{(g_C)}$  adding new observations
17:  end for
18: end function

```

BO and CBO methods [Hernández-Lobato et al., 2014, 2015, Wang and Jegelka, 2017]. In the RFF-based sampling, RFF $\phi(\mathbf{x}) \in \mathbb{R}^D$ are first generated, and a Bayesian linear regression model $f(\mathbf{x}) \approx \boldsymbol{\omega}^\top \phi(\mathbf{x})$ with the coefficients $\boldsymbol{\omega} \in \mathbb{R}^D$ is constructed. By sampling the coefficients $\boldsymbol{\omega}$ from the Gaussian posterior, a continuous sample path can be derived. Let $\tilde{f}_{(k)}$ and $\tilde{g}_{c(k)}$ ($c \in \{1, \dots, C\}$) be the k -th set of sample paths ($k \in \{1, \dots, K\}$) for the objective and constraint functions. The k -th sample of f_* , can be obtained by solving a constrained optimization problem $\max_{\mathbf{x} \in \mathcal{X}} \tilde{f}_{(k)}(\mathbf{x})$, s.t. $\tilde{g}_{c(k)}(\mathbf{x}) \geq z_c$, $c = 1, \dots, C$. We can apply any constrained optimization modules such as the method of moving asymptotes [Svanberg, 2002]. Another approach would be the discretization-based sampling through multivariate normal distribution [Perrone et al., 2019], though the number of discretization points strongly depends on the input dimension d for sufficiently accurate sampling.

For parallel querying, we need to sample the f_* and \mathcal{H}_{q-1} simultaneously. By using RFF-based sampling, these random variables are sampled from a joint distribution easily, i.e., \mathcal{H}_{q-1} can be sampled as a value of the sample paths $\tilde{f}_{(k)}(\mathbf{x})$ and $\tilde{g}_{c(k)}(\mathbf{x})$ at $\mathbf{x} \in \mathcal{X}_{q-1}$. Moreover, in the MC approximation for $q > 1$, we can reuse the sample paths $\tilde{f}_{(k)}, \tilde{g}_{1(k)}, \dots, \tilde{g}_{C(k)}$ that are sampled at $q = 1$ as described in Algo. 1. Because of this reuse, the computational cost of parallel CMES and CMES-IBO are much smaller than Q times that of

sequential CMES and CMES-IBO, respectively.

H.2 Computational Complexity of CMES-IBO and CMES

Independent Case To generate sample paths, the Bayesian linear regression requires $O(CKD^3)$ for the given RFF, but C , K and D are usually not large values. The number of constraints C is often less than 10. In our empirical observations, the performance of CMES-IBO were stable with a small number of MC samplings K such as 10. The dimension of the RFF features D is typically set as less than 1000. The complexity for solving the generated constraint problems depends on the solver. Many gradient-based methods have been known for the white-box constrained optimization such as the sequential quadratic programming and the interior point method. The gradient of a sample path can be obtained by $O(dD)$, and thus, those gradient-based solvers can be applied efficiently.

Once we obtain the samples of f_* , the acquisition functions CMES-IBO (7) and CMES (11) can be easily calculated for $\forall \mathbf{x}$ by using the GP posterior of f and g_c . Since we employ a standard GP model, the posterior can be computed with $O(n^3)$ for a given kernel matrix, where n is the number of the observed points. Note that the $O(n^3)$ computation is required only once through the acquisition function maximization, because by storing $(\mathbf{K} + \sigma_{\text{noise}}^2 \mathbf{I})^{-1}$, the predictive mean and variance can be evaluated by $O(n^2)$ for a given \mathbf{x} . In our setting, the function evaluation is assumed to be expensive, by which we usually only have a moderate size of a training set (typically, at most several hundreds of points).

In the case of the parallel setting, we need $m_q^{(f)}$ and $s_q^{(f)2}$, which are the predictive mean and variance of $f(\mathbf{x})$ after conditioning \mathcal{H}_{q-1} . This conditional density is written as $p(f(\mathbf{x}) | \tilde{f}_{(k)}(\mathbf{x}^{(1)}), \dots, \tilde{f}_{(k)}(\mathbf{x}^{(q-1)}))$, which can be easily determined through the standard conditional Gaussian formula. Given the $q \times q$ predictive covariance matrix of the current GP for \mathbf{x} and \mathcal{X}_{q-1} , we can obtain $m_q^{(f)}(\mathbf{x})$ and $s_q^{(f)2}(\mathbf{x})$ with $O(q^3)$. For $m_q^{(g_c)}$ and $s_q^{(g_c)2}$, which are for constraint functions, the same calculation can be applied.

Correlated Case For CMES-IBO and CMES, the computations of CDF of the multivariate normal distribution are needed in the correlated case, as shown in Appendix G.2. CMES-IBO performs K times $C + 1$ dimensional CDF for the acquisition function (7), in which $Z = \Pr(\mathbf{h} \in \mathcal{A}_{f_*})$ is now CDF of a correlated multivariate normal distribution. On the other hand, in addition to these CDF computations, CMES performs K times computations of the expectation and covariance matrix of TMN in the acquisition function (20), each of which needs computing C dimensional CDF $C + 1$ times and $C - 1$ dimensional CDF $C(C+1)/2$ times, respectively [G and Wilhelm, 2012]. Using a well-known MC-based algorithm [Genz, 1992], the computational complexity of CDF with respect to the dimension C is known to be $O(C^2)$. Therefore, the computational complexity of CMES-IBO with respect to K and C is $O(KC^2)$, but that of CMES is $O(KC^4)$, which severely limits the applicability of CMES to the large number of constraints.

I Considerations on Regret Bound of MES

In this section, we describe flaws in the theoretical analysis of MES [Wang and Jegelka, 2017]. We use the same notation as [Wang and Jegelka, 2017] throughout this section. Wang and Jegelka [2017] showed the bound of simple regret $r_T := \max_{\mathbf{x} \in \mathcal{X}} f(\mathbf{x}) - \max_{t \in [1, T]} f(\mathbf{x}_t)$ as follows:

Theorem I.1 (Theorem 3.2 in [Wang and Jegelka, 2017]). *Let F be the cumulative probability distribution for the maximum of any function f sampled from $GP(\mu, k)$ over the compact search space $\mathcal{X} \subset \mathbb{R}^d$, where $k(\mathbf{x}, \mathbf{x}') \leq 1, \forall \mathbf{x}, \mathbf{x}' \in \mathcal{X}$. Let $f_* = \max_{\mathbf{x} \in \mathcal{X}} f(\mathbf{x})$ and $w = F(f_*) \in (0, 1)$, and assume the observation noise is iid $\mathcal{N}(0, \sigma^2)$. If in each iteration t , the query point is chosen as $\mathbf{x}_t = \arg \max_{\mathbf{x} \in \mathcal{X}} \gamma_{y_*^t}(\mathbf{x}) \frac{\psi(\gamma_{y_*^t}(\mathbf{x}))}{2\Psi(\gamma_{y_*^t}(\mathbf{x}))} - \log(\Psi(\gamma_{y_*^t}(\mathbf{x})))$, where $\gamma_{y_*^t}(\mathbf{x}) = \frac{y_*^t - \mu_t(\mathbf{x})}{\sigma_t(\mathbf{x})}$ and y_*^t is drawn from F , then with probability at least $1 - \delta$, in $T' = \sum_{i=1}^T \log_w \frac{\delta}{2\pi_i}$ number of iterations, the simple regret satisfies*

$$r_{T'} \leq \sqrt{\frac{C\rho_T}{T}}(\nu_{t^*} + \zeta_T), \quad (25)$$

where $C = 2/\log(1+\sigma^{-2})$ and $\zeta_T = (2\log(\frac{\pi_T}{\delta}))^{\frac{1}{2}}$, π_i satisfies $\sum_{i=1}^T \pi_i^{-1} \leq 1$ and $\pi_i > 0$, and $t^* = \arg \max_t \nu_t$ with $\nu_t \triangleq \min_{\mathbf{x} \in \mathcal{X}, y_*^t > f_*} \gamma_{y_*^t}(\mathbf{x})$, and ρ_T is the maximum information gain of at most T selected points.

In this theorem, the simple regret for ‘one sample MES’ is analyzed, in which only one max-value is sampled at every iteration in the algorithm. We summarize five main flaws in this theorem as follows (note that each of them is related to each other):

1. From the assumption $f \sim \mathcal{GP}(\mu, k)$, the max-value f_* is a random variable, but it is not treated as a random variable in their analysis. For example, Lemma C.1 in [Wang and Jegelka, 2017] obviously assumes that $f(\mathbf{x}_t)$ follows the Gaussian distribution, and therefore, treating f_* as a deterministic variable contradicts the assumption of this lemma. This problem closely related to other flaws, and thus, it is difficult to correct.
2. In BO literature, usually, the number of iterations is represented by T , and Wang and Jegelka [2017] use this notation except for the theorem. On the other hand, in the theorem, the number of iteration is represented by T' instead of T , and the variable T in the bound (25) is defined by the number of ‘partitioning’ of the entire iterations in their proof. Each partition is defined so that it satisfies a probabilistic condition related to max-values, which we omit details here. An important issue is that, for this replaced T , dependency on the actual number of iterations is not clarified. Therefore, (25) does not reveal the convergence rate with respect to the number of iterations.
3. Since ν_{t^*} depends on y_*^t in each iteration, ν_{t^*} is a random variable. This variable remains in the final upper bound, but the convergence rate of ν_{t^*} has not been shown.
4. In the theorem, Wang and Jegelka [2017] assumed that y_*^t is drawn from the prior F . This assumption clearly does not match the basic idea of MES that selects the next query based on the mutual information estimated through samples of the max-value from the ‘posterior’ distribution.

5. Wang and Jegelka [2017] claimed that the above simple regret bound can adapt to the setting that y_*^t is drawn from the posterior. However, this claim is not proven and not obvious. In the proof, Wang and Jegelka [2017] implicitly assumed $\Pr(y_*^t < f_*, y_*^{t+1} < f_*) = \Pr(y_*^t < f_*)\Pr(y_*^{t+1} < f_*)$. Through the basic formula of the joint probability of independent variables, this decomposition is allowed if f_* is deterministic, and y_*^t and y_*^{t+1} are independent of each other. However, both of these two conditions are not satisfied in the case of sampling from the posterior. For the first condition, as we already mention, f_* should be a random variable (actually, this first condition is not satisfied even for the case of sampling from the prior). For the second condition, when y_*^t and y_*^{t+1} are sampled from posterior, y_*^t depends on \mathcal{D}_{t-1} and y_*^{t+1} depends on \mathcal{D}_t . However, since $\mathcal{D}_{t-1} \subset \mathcal{D}_t$, dependency obviously exists between y_*^t and y_*^{t+1} (note that now \mathcal{D}_{t-1} and \mathcal{D}_t are also random variables not only because of the random noise of observations, but also the randomness in the acquisition function). In the proof, the decomposition is not justified when the two conditions are not satisfied. This decomposition plays a key role in the proof, and we consider that the above issue is not easy to avoid.

We first tried to extend this theorem to our constrained problem, but we consider that correcting the above issues is at least not trivial. Therefore, theoretical analysis of the MES-based methods (even for the simple unconstrained case) is still an open problem, to the best of our knowledge.

J Details of Experimental Settings

In this section, we describe additional details of experimental settings.

J.1 Other Experimental Settings

Observations for objective and constraint functions are standardized so that they have zero mean and unit variance, respectively, before the regression at every iteration. We used the open-source library called GPpy [GPpy, since 2012] for the GP regression. The candidate intervals of hyperparameters σ_{LIN}^2 and σ_{RBF}^2 are set to $[0, 1]$, and the variance of the noise σ^2 is set to 10^{-6} . As we mentioned in the main paper, other hyperparameters are chosen by marginal likelihood maximization. We employed an Automatic Relevance Determination (ARD) for the RBF kernel. Thus, the RBF kernel has a hyperparameter $\boldsymbol{\ell} := (\ell_1, \dots, \ell_d)^\top \in \mathbb{R}^d$, and it is written as

$$k_{\text{RBF}}(\mathbf{x}, \mathbf{x}') := \exp\left(-\frac{1}{2} \sum_{i=1}^d \frac{(x_i - x'_i)^2}{\ell_i^2}\right),$$

where x_i and x'_i are the i -th elements of \mathbf{x} and \mathbf{x}' , respectively. For each one of ℓ_i for $i = 1, \dots, d$, we set the same interval of the candidate value. For the benchmark functions and the real-world function, we set $\ell_i \in [10^{-1}s_i, 10s_i]$, where s_i is the length of the interval for the possible value of x_i in the input domain. For all benchmark functions and real-world function, $z_c = 0$ for $c = 1, \dots, C$. We used the method of moving

asymptotes [Svanberg, 2002] in NLopt [Johnson, since 2008] for the constrained optimization of the sample path in CMES-IBO, CMES, TSC, and their parallel extensions. The number of initial points are set as 3 for the GP-derived synthetic function, 5 for the two-dimensional benchmark functions, $5d$ for the Hartmann6 function, and 25 for others. Finally, the hyperparameter M of P-EIC is selected as the minimum of the current observations.

J.2 Details of Benchmark Functions

Here, we provide detailed information on benchmark functions. Note that we change the sign from the original functions if it is required to formalize as the maximization problem.

Gardner1 Gardner1 is a simple test problem in which functions are constructed by sine and cosine functions [Gardner et al., 2014]. The input dimension $d = 2$, the input domain $\mathcal{X} = [0, 6]^2$, and the number of constraints $C = 1$. The detailed forms of functions are

$$\begin{aligned} f(\mathbf{x}) &= -\cos(2x_1)\cos(x_2) - \sin(x_1), \\ g_1(\mathbf{x}) &= -\cos(x_1)\cos(x_2) + \sin(x_1)\sin(x_2) + 0.5. \end{aligned}$$

Gardner2 Gardner2 also has a simple form, but its feasible region is very small [Gardner et al., 2014]. The input dimension $d = 2$, the input domain $\mathcal{X} = [0, 6]^2$, and the number of constraints $C = 1$. The detailed forms of functions are

$$\begin{aligned} f(\mathbf{x}) &= -\sin(x_1) - x_2, \\ g_1(\mathbf{x}) &= -\sin(x_1)\sin(x_2) - 0.95. \end{aligned}$$

Gramacy The Gramacy function is from [Gramacy et al., 2016]. The input dimension $d = 2$, the input domain $\mathcal{X} = [0, 1]^2$, and the number of constraints $C = 2$. The detailed forms of functions are

$$\begin{aligned} f(\mathbf{x}) &= -x_1 - x_2, \\ g_1(\mathbf{x}) &= \frac{1}{2}\sin(2\pi(x_1^2 - 2x_2)) + x_1 + 2x_2 - 1.5, \\ g_2(\mathbf{x}) &= -x_1^2 - x_2^2 + 1.5. \end{aligned}$$

Hartmann6 The Hartmann6 function is used in [Letham et al., 2019]. The input dimension $d = 6$, the input domain $\mathcal{X} = [0, 1]^6$, and the number of constraints $C = 1$. The detailed forms of functions are

$$\begin{aligned} f(\mathbf{x}) &= \sum_{i=1}^4 \alpha_i \exp\left(-\sum_{j=1}^6 A_{ij}(x_j - P_{ij})^2\right), \\ g_1(\mathbf{x}) &= -\|\mathbf{x} - \mathbf{x}'\| + 1, \end{aligned}$$

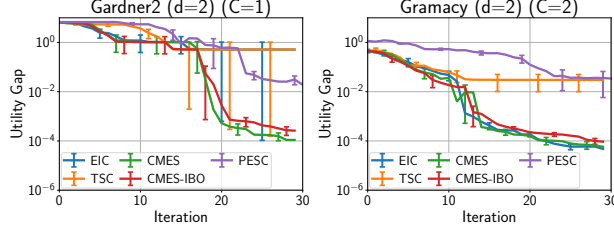


Figure 6: Utility gap of small C benchmark functions (average and standard error).

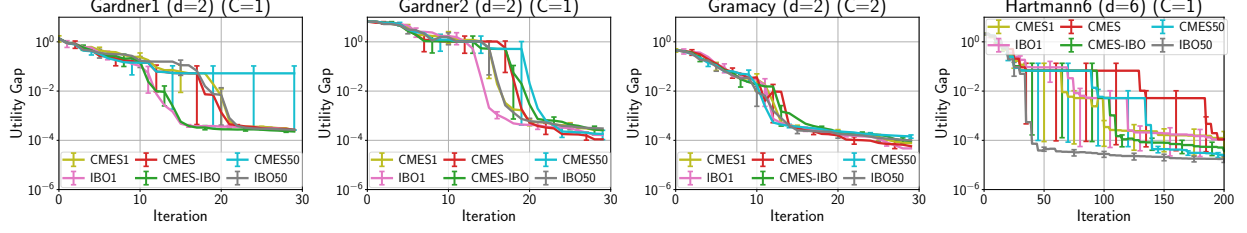


Figure 7: Utility gap of small C benchmark functions with different K (average and standard error).

where

$$\alpha = (1.0, 1.2, 3.0, 3.2)^\top,$$

$$\mathbf{A} = \begin{pmatrix} 10 & 3 & 17 & 3.5 & 1.7 & 8 \\ 0.05 & 10 & 17 & 0.1 & 8 & 14 \\ 3 & 3.5 & 1.7 & 10 & 17 & 8 \\ 17 & 8 & 0.05 & 10 & 0.1 & 14 \end{pmatrix},$$

$$\mathbf{P} = 10^{-4} \begin{pmatrix} 1312 & 1696 & 5569 & 124 & 8283 & 5886 \\ 2329 & 4135 & 8307 & 3736 & 1004 & 9991 \\ 2348 & 1451 & 3522 & 2883 & 3047 & 6650 \\ 4047 & 8828 & 8732 & 5743 & 1091 & 381 \end{pmatrix}.$$

K Additional Experiments

K.1 Experiments on Small C Problems

Here, we show the experimental results of small C benchmark functions in Fig. 6. In the sequential querying for additional benchmarks, called Gardner1 and Gramacy, CMES and CMES-IBO shows superior performance. In particular, the result of Gardner2, which has a tiny feasible region, implies that entropy-based methods, including CMES-IBO, could find the small feasible region.

Further, we show the results with different $K = 1, 50$ in Figure 7, where the suffix number of the method name means K . In this figure, CMES and CMES-IBO with $K = 10$ are also plotted for comparison. We can see that both methods were not changed a lot depending on K , which implies the robustness regarding K .

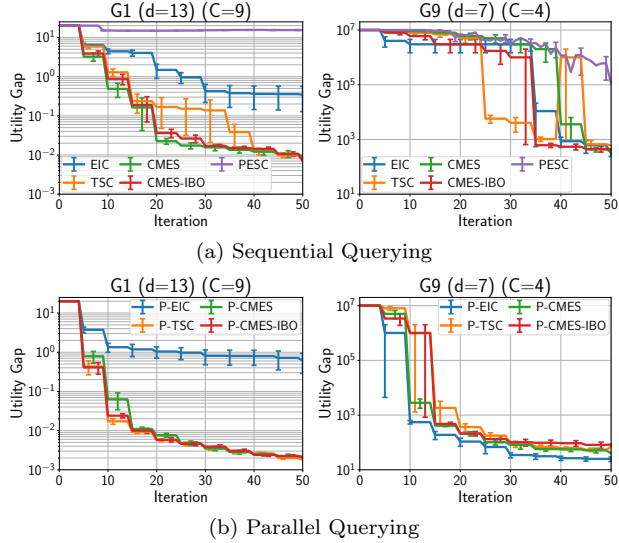


Figure 8: Utility gap of G1 and G9 functions (average and standard error).

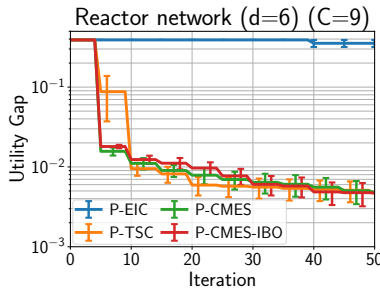


Figure 9: Utility gap of the real-world problem for the parallel setting (average and standard error).

K.2 Experiments on Large C Problems

The results on the two benchmark functions called G1 ($d = 13$ and $C = 9$) and G9 ($d = 7$ and $C = 4$) are shown in Fig. 8. For the sequential querying, CMES-IBO was the best or comparable to the best methods in both results. In G9, TSC decreased the gap rapidly, but it showed the unstable behavior from the iterations around 40 to 45. We consider that these unstable behavior stem from the stochastic nature of TSC. EIC was slow for G1 though it shows reasonable performance for G9. For the parallel querying, CMES-IBO again showed stable performance, though most of the methods have similar performance in these cases.

K.3 Experiments on Real-World Problem for the Parallel Setting

Figure 9 shows the results of the real-world problem for the parallel setting. Except for P-EIC, all methods are accelerated by parallelization, and CMES-IBO shows comparable performance to the best result.

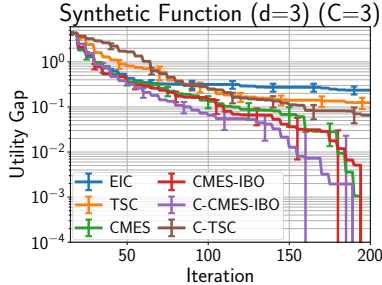


Figure 10: Utility gap of correlated GP-derived synthetic functions (average and standard error).

K.4 Experiment for Correlated Synthetic Function

We evaluate the performance of CMES-IBO with correlated GPs on synthetic functions ($d = 3$ and $C = 3$). Because of its high computational complexity, we did not employ CMES here (see Appendix H.2). The objective and $C = 3$ constraints were sampled from GPs with the RBF kernel, and the length scales of the kernels were 0.1. All the correlation coefficients among the objective and constraint functions were set as 0.5. The same settings of GPs for the function generation were also used in each BO method. The number of initial points is set as 5. The threshold for constraints were set as $z_c = 0$ for $\forall c$, and the input domain was $[0, 1]^3$. We sampled 5 sets of functions, and the experiment of each set ran 10 times. We report the mean and standard error of these 50 trials. Figure 10 shows the result. C-CMES-IBO denotes the correlated extension of CMES-IBO. We see that C-CMES-IBO improves CMES-IBO in this case and is superior to the other methods. Although the correlated model can improve performance when the true function has a strong correlation, we mainly focus on the independent setting because the efficiency is often comparable to the correlated model, and the computations of independent CMES-IBO is much simpler than correlated case.

K.5 Experiment for Computational Time Evaluation

In Table 1, we evaluate computational time of the acquisition function maximization at $t = 30$. EIC and TSC were relatively faster than the others. CMES-IBO and CMES took longer times because of sampling of f_* for which we need to solve constraint optimization problems K times, while the acquisition function maximization itself was fast enough because of their simple closed forms of the acquisition functions. Although it is not shown here, PESC has the same computational requirement for sampling x_* because the same constraint optimization problems need to be solved. It is worth noting that the K times sampling of f_* can be accelerated by computing in parallel because each one of the samplings is independent.

Table 1: Computational time (sec.) for the Gramacy function at $t = 30$ (mean \pm standard error)

	sampling of f_*	optimization of $\alpha(\boldsymbol{x})$
EIC	NA	1.148 ± 0.287
TSC	NA	2.670 ± 0.464
CMES	20.728 ± 1.498	0.780 ± 1.317
CMES-IBO	21.836 ± 0.933	1.163 ± 2.130